THE GEOLOGICAL SOCIETY OF AMERICA®

# A lithostratigraphic and magnetostratigraphic framework in a geochronologic context for a purported Permian–Triassic boundary section at Old (West) Lootsberg Pass, Karoo Basin, South Africa

**Robert A. Gastaldo[1,†], Johann Neveling[2,†], John W. Geissman[3,†], and Sandra L. Kamo[4,†]**
[1]*Department of Geology, Colby College, Waterville, Maine 04901, USA*
[2]*Council for Geosciences, Private Bag x112, Silverton, Pretoria, 0001, South Africa*
[3]*Department of Geosciences, ROC21, The University of Texas at Dallas, Richardson, Texas 75080-3021, USA*
[4]*Jack Satterly Geochronology Laboratory, University of Toronto, Toronto, Ontario, M5S 3B1, Canada*

## ABSTRACT

**Current models of the terrestrial biosphere's response to the end-Permian crisis are based largely on lithostratigraphic, magnetostratigraphic, and biostratigraphic records obtained from sedimentary successions in the Karoo Basin, South Africa. These successions have been interpreted to represent continuous sedimentation across the upper *Daptocephalus* and lower *Lystrosaurus* vertebrate-assemblage zones, assigned to the Elandsberg Member and lower Palingkloof Member, and upper Palingkloof Member and overlying Katberg Formation, respectively. The stratigraphic section at Old (West) Lootsberg Pass, Eastern Cape Province, is used as a cornerstone for the currently accepted model correlated with the marine extinction event, in part, based on a magnetic polarity stratigraphy of limited documentation. Our current multidisciplinary effort provides a refined stratigraphic framework, encompassing over 740 m of measured section, compiled from 12 closely spaced and physically correlated localities across a northwest-to-southeast distance of less than 2 km. This framework is placed into magnetostratigraphic context and constrained by U-Pb isotope dilution–thermal ionization mass spectrometry (ID-TIMS) results for two horizons.**

**The Old Lootsberg Pass succession does not record continuous sedimentation, as previously argued. Rather, the presence of several intraformational pedogenic-nodule conglomerate-lag deposits, a character used by other workers as diagnostic of the Katberg Formation, occurs in the Elandsberg Member ~100 m stratigraphically below the Katberg Formation. An interlaminated lithofacies, previously used as a diagnostic feature of the terrestrial extinction event, occurs isolated at several stratigraphic positions, indicating that it is neither unique nor mappable. A dominant signature of normal-polarity magnetozones in the section is interrupted by two, short, reverse-polarity intervals that are restricted to siltstone beneath erosional contacts with fluvial sandstones, indicating their cryptic nature in the succession. In addition, we report a Wuchiapingian maximum-age estimate for a detrital zircon population from a bed stratigraphically above a previously reported Early Changhsingian age estimate for these rocks. A comparison of the sedimentologic features of these deposits reveals that the bed from which the Changhsingian age is derived supports an ashfall interpretation rather than a reworked deposit from which the Wuchiapingian depositional age is derived. A synthesis of our observations from Old (West) Lootsberg Pass with global patterns reported from the marine realm leads to the conclusion that the turnover from the *Daptocephalus* to *Lystrosaurus* Assemblage Zones is not coincident with the end-Permian marine event. Hence, our results demonstrate that geochronometric constraints, where available, and a high-resolution sampling strategy for paleomagnetic context are essential to any research program when attempting to interpret patterns of biological turnover, replacement, and extinction in continental successions.**

## INTRODUCTION

The end-Permian mass extinction, dated at 251.9 Ma in the marine section at Meishan, China (Burgess et al., 2014; Baresel et al., 2017), is reported as a synchronous event in the marine and terrestrial realms (Twitchett et al., 2001; Ward et al., 2005; Shen et al., 2011), that played out over a 60 ± 48 ka interval. Estimates of marine-biodiversity loss approach 85 percent (Clapham and Payne, 2011), with different clades experiencing dissimilar extinction rates over variable time scales. In contrast, terrestrial vertebrate extinction is reported to have affected 63 percent of families in which 89 percent of tetrapod genera were lost (Benton and Newell, 2014) over a time interval estimated to have lasted less than 120 ka (Smith and Botha-Brink, 2014). The one major plant clade that is believed to have experienced wholesale extinction is the southern hemisphere Glossopteridales (Benton and Newell, 2014; although see Gastaldo et al., 2015, 2017). The demise of this wetland ecosystem is thought to be associated with ecological instability and pre- or coincident collapse of plant communities in response to the crisis (McElwain and Punyasena, 2007). As such, this "Mother of Mass Extinctions" (Erwin, 2006) is used as a model for ecosystem response to severe perturbation, and is considered a possible scenario for how Earth systems may react to current, rapid global warming and climate extremes (Payne and Clapham, 2012; Benton and Newell, 2014).

The current idea of a phased, end-Permian loss in vertebrate biodiversity is interpreted, in large part, from the biostratigraphic record of the fully terrestrial succession exposed in the fully continental Karoo Basin, South Africa (although see Marshall, 2005; Lucas, 2017a, 2017b). Here, the extinction event is believed to be preserved in the basin's lithostratigraphic record and has long been considered to be the point at which vertebrate biozones turnover from the *Daptocephalus* (formerly *Dicynodon*; Viglietti et al., 2016, 2018) to the *Lystrosaurus* Assemblage Zone (Ward et al., 2005; Smith and Botha-Brink, 2014) in what is considered the Lootsbergian Land Vertebrate Faunachron

[†]ragastal@colby.edu, jneveling@geoscience.org.za, geissman@utdallas.edu, skamo@es.utoronto.ca.

*GSA Bulletin*; https://doi.org/10.1130/B31881.1; 19 figures; 1 table; Data Repository item 2018119.

(Lucas, 2010). The demise of the vertebrate fauna purportedly was accompanied by catastrophic, basin-wide vegetational die off (Ward et al., 2000, 2005; Rubidge et al., 2016) associated with the onset of extreme drought (Smith and Ward, 2001), and followed by a rapid recovery of vertebrates in the earliest Triassic (Botha and Smith, 2006; Roopnarine et al., 2007; Sidor et al., 2013; Smith and Botha-Brink, 2014; Roopnarine and Angielczyk, 2015). The extinction-and-recovery model is based on the premise that lithologic features of the rocks in which the vertebrates are preserved in an almost continuous record across this critical interval in Earth history (Smith, 1995; Ward et al., 2005; Smith and Botha, 2005; Smith and Botha-Brink, 2014; Viglietti et al., 2016; Rubidge et al., 2016). Hence, vertical stratigraphic changes across this interval are reported to reflect the crisis, and are interpreted based: on siltstone color, a change from olive-gray to mottled to grayish-red siltstone; and fluvial architectural elements, from sandstone bar forms associated with high sinuosity rivers to those characteristic of anabranching systems in which intraformational pedogenic nodule conglomerate is found (Pace et al., 2009). These landscape changes are interpreted to reflect part of a global response to changing climate (Ward et al., 2000; Benton and Newell, 2014), from humid temperate to semi-arid conditions (Smith and Botha-Brink, 2014) that resulted in ecosystem perturbation. Currently, 11 localities in which the vertebrate-defined Permian–Triassic boundary (PTB) is reported comprise the focus of relatively recent South African studies (Ward et al., 2005; Smith and Botha-Brink, 2014; Botha-Brink et al., 2014). In the Free State Province these are Bethulie, Caledon, Fairydale, and Nooitgedacht 68. The localities in the Eastern Cape Province are Carlton Heights, Commandodrift, Wapadsberg Pass, (East) Lootsberg Pass, Tweefontein, Old (West) Lootsberg Pass (Fig. 1), and Ripplemead. Despite the number of localities where the vertebrate-defined boundary is inferred, no physical datum exists on which the PTB can be identified at, or correlated among, localities throughout the basin (Gastaldo et al., 2009, 2017; Gastaldo and Neveling, 2012, 2016; Neveling et al., 2016a, 2016b). In addition, no facies relationships are published for any one of these localities that demonstrate their uniqueness. And, although both a chemostratigraphy (MacLeod et al., 2000) and magnetostratigraphy (Ward et al., 2005) have been proposed, neither has been able to be replicated in subsequent investigations (Gastaldo et al., 2014, 2015) and correlated with the marine record.

Old (West) Lootsberg Pass is one of the foundational localities on which the end-Permian

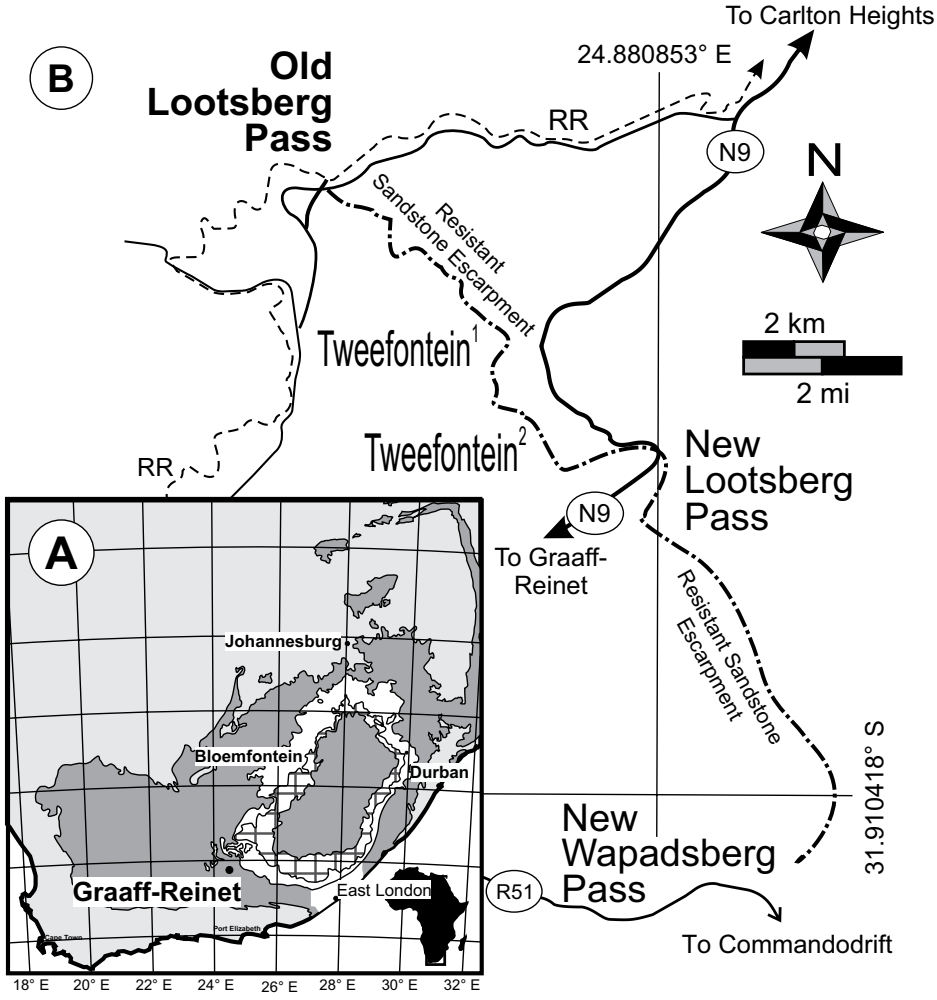


**Figure 1. Locality maps. (A) Generalized map of South Africa with an outline of the Karoo Basin in dark gray onto which the distribution of rocks hosting the *Daptocephalus* (white polygon; Viglietti et al., 2016) and *Lystrosaurus* (hatched; Rubidge, 1995) Assemblage Zones are shown. (B) Four localities in the Eastern Cape Province–Wapadsberg Pass, (New) Lootsberg Pass, Tweefontein, and Old (West) Lootsberg Pass–reported as foundational to the terrestrial, end-Permian extinction model (Ward et al., 2000, 2005; Smith and Botha-Brink, 2014). The current study focuses on Old Lootsberg Pass in bold.**

terrestrial extinction model in the Karoo Basin is based (Ward et al., 2000; Smith and Ward, 2001; Ward et al., 2005). The widely accepted vertebrate biostratigraphic paradigm has been reported in a generalized, composite stratigraphic section at this locality which is accompanied by a magnetic polarity stratigraphy, interpreted as being able to be correlated with a magnetic polarity time scale as defined by data from coeval marine successions (Ward et al., 2005). Here, we present the first multidisciplinary litho- and magnetostratigraphic framework in a chronostratigraphic context for a South African succession at the Old (West) Lootsberg Pass locality that transitions the vertebrate biozones (Gastaldo et al., 2017) purported as the equivalent to the end-Permian marine extinction. Our data indicate that criteria currently used to discriminate reportedly Permian and Triassic rocks are lateral equivalents across a short geographic distance, and that the transition from the *Daptocephalus* to *Lystrosaurus* Assemblage Zone is likely within the early Changhsingian stage rather than across the Changhsingian to Induan as interpreted (Gastaldo et al., 2017).

### *Daptocephalus* and *Lystrosaurus* Assemblage Zone Landscapes

Latest Permian (Lopingian) strata are assigned to the Middleton and Balfour formations (Rubidge et al., 2013), with the latter compris-

ing five formal members that include, in stratigraphic order, the Ouedeberg, Daggaboersnek, Barberskrans, Elandsberg, and Palingkloof members (Fig. 2). Wuchiapingian rocks are overlain by Changhsingian deposits probably in the Barberskrans Member of the Balfour Formation. This transition is based on a recently published U-Pb isotope dilution–thermal ionization mass spectrometry (ID-TIMS) Early Changhsingian age (253.48 ± 0.15 Ma) from a silicified porcellanite on the Blaauwater 65 Farm at Old (West) Lootsberg Pass (Fig. 3; Gastaldo et al., 2015). Traditionally, and based largely on Broom's (1906, 1911) assumption, the *Daptocephalus* (formerly *Dicynodon*; Viglietti et al., 2016) biozone is considered as latest Permian and the overlying *Lystrosaurus* biozone is earliest Triassic in age (Smith, 1995; Ward et al., 2000; Smith and Ward, 2001; Ward et al., 2005; Smith and Botha-Brink, 2014, and others). An early Triassic age has been assigned to the uppermost exposures of the Palingkloof Member and overlying Katberg Formation. Gastaldo et al. (2015) and Neveling et al. (2016a, 2016b) argue that either the Permian–Triassic boundary must be preserved higher in the Katberg Formation or entirely missing, a situation similar to that reported at Senekal in the Free State where the succession is condensed and a significant diastem exists (Hancox et al., 2002).

Sedimentary rocks that represent former land surfaces of the *Daptocephalus* and *Lystrosaurus* biozones are very similar. Fine-grained, olive-gray and reddish-gray siltstones are most common, and both are interpreted to represent paleosols (Smith, 1995; Gastaldo et al., 2014) and abandoned channel-fills (Gastaldo et al., 2009; Gastaldo and Neveling, 2012; Li et al., 2017). Olive-gray siltstone predominates in the Elandsberg Member, whereas reddish-gray mottling is also found locally (Neveling et al., 2016a). The frequency of reddish-gray siltstone is reported to increase stratigraphically higher in the upper Palingkloof Member and overlying Katberg Formation (Smith, 1995; Johnson et al., 2006). Although roughly generalized in recent literature as containing predominantly monotonous maroon siltstone paleosols with calcretes in a sandstone-dominated interval (Ward et al., 2000; Smith and Ward, 2001), siltstones of the Katberg Formation exhibit the full range of colors and color combinations from light olive-gray and olive-gray through mottling with dusky red to reddish-gray (Hiller and Stavrakis, 1980, 1984; Retallack et al., 2003; Gastaldo and Rolerson, 2008; Li et al., 2017). Channel-bedload deposits also are compositionally similar in both assemblage zones, and consist of grayish-yellow, fine- to very fine-grained feldspathic or lithic wacke. These lithologies are organized into low-angle and trough crossbed sets of thicknesses ranging from <20 to >50 cm and several geometries (Pace et al., 2009), with a reported changeover in fluvial regime. Sandstone bodies in the older *Daptocephalus* biozone are reported to represent deep and meandering fluvial geometries whereas those characterizing the *Lystrosaurus* biozone are interpreted as anabranching (braided) regimes (Hancox et al., 2002; Ward et al., 2000, 2005).

Fluvial architectures of the Katberg Formation are reported as shallow, broad channels in which basal channel-lag deposits overlie deep erosional surfaces (Neveling, 2004; Pace et al., 2009). In conjunction with thick, amalgamated sandstone bodies, channel lags and trough fills are characterized by the presence of: (1) intraformational clast- or matrix-supported, pedogenic nodular conglomerates (PNC), considered by other workers as a diagnostic feature of the basal Katberg Formation (Botha and Smith, 2006; Smith and Botha-Brink, 2014); and (2) intraformational mud-chip conglomerate with mudclast aggregates (Pace et al., 2009; Gastaldo et al., 2013). The overall character of the lower Katberg fluvial facies varies spatially depending on proximity to the Cape Fold Belt to the south and east. Channel geometries in localities distal to the Cape Fold Belt (e.g., Carlton Heights) are sheet-like and thin (generally 5–6 m), may extend laterally over a few hundred meters, show evidence of subaerial exposure on barform crests, and are multistoried due to their amalgamation and stacking as a result of extreme landscape degradation (Pace et al., 2009; Gastaldo et al., 2013). At localities in more proximal settings, closer to the Cape Fold Belt, multistory channels are thicker (>10 m; Hiller and Stavrakis, 1984) and can be traced laterally for distances of several kilometers along strike. These deposits may contain both intraformational and extraformational (igneous, metamorphic, and sedimentary) clasts (Hiller and Stavrakis, 1980, 1984). Here, the proportion of sandstone to siltstone is higher than in distal sections, stacked barforms rarely show trough fills of mudchip conglomerate, and channel bases may contain localized PNC lags.

Pedogenic calcite-cemented nodules in PNCs are the remnants of paleo-Vertisols or paleo-Calcisols that accumulated during landscape degradation (Pace et al., 2009). These lag deposits are reported to be a characteristic of river channels of the *Lystrosaurus* biozone, believed to be diagnostic of the Katberg Formation, and are interpreted to indicate an important change in the effect of climate on the Karoo landscape (Botha and Smith, 2006; Smith and Botha-Brink, 2014). Their presence is interpreted to reflect a shift from seasonally wet conditions of the *Daptocephalus* Assemblage Zone, in which reducing paleosols with high water tables predominated (Prevec et al., 2010; Gastaldo et al., 2014), to a more seasonally dry climate in the *Lystrosaurus* biozone, in which wetland paleosols (Gastaldo and Rolerson, 2008) matured resulting in calcic-Vertisol overprinting. Subsequently, calcic-Vertisols were scavenged when the climate shifted back to more seasonally wet conditions, concentrating the larger clasts either at the base of channels or as isolated lenticular deposits in the alluvial floodplain (Pace et al., 2009). In the Bethulie section, distal to the Cape Fold Belt, lenticular PNC deposits are described as isolated in siltstone and as lags in thin ribbon (<3 m) sandstone bodies (Smith, 1995; Botha and Smith, 2006). These are assigned to the informal, upper Palingkloof Member and considered as precursor to the arrival of the Katberg fluvial regimes (Ward et al., 2000).

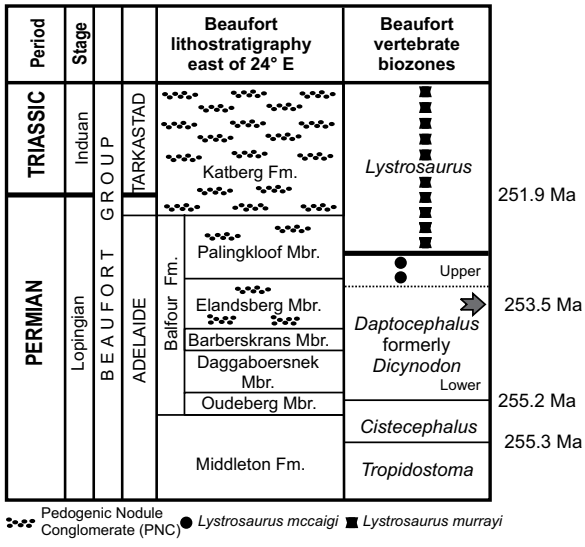


**Figure 2. Generalized stratigraphy of the Beaufort Group, Karoo Basin, South Africa, including lithostratigraphic units (following Johnson et al., 2006), biostratigraphic Vertebrate Assemblage Zones (Rubidge, 1995; Viglietti et al., 2016), Assemblage Zone boundary ages (after Rubidge et al., 2013; Burgess et al., 2014), and stratigraphic position of reported U-Pb ID-TIMS age of Gastaldo et al. (2015) at arrow in the Elandsberg Member.**

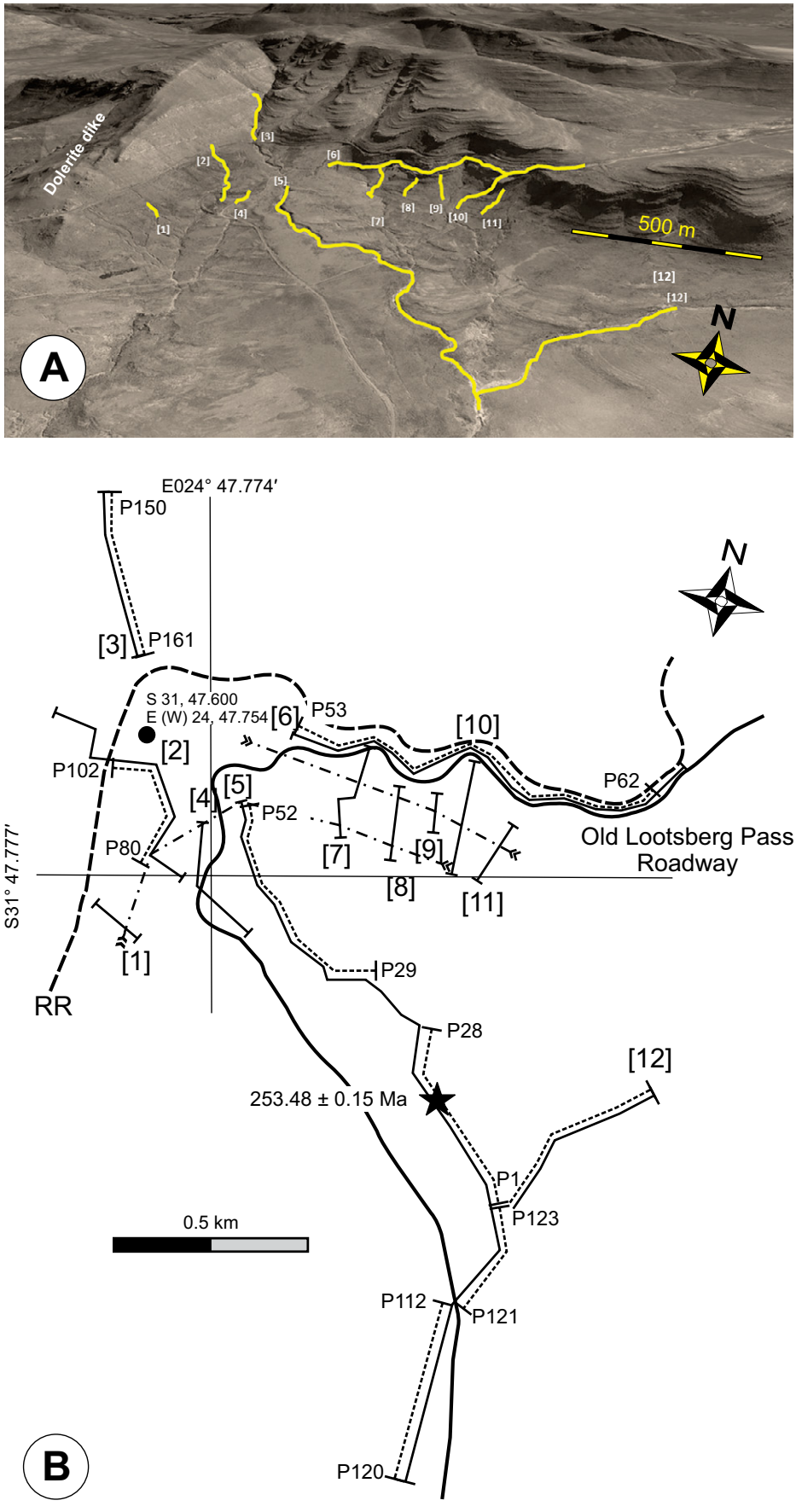


**Figure 3. Measured sections at Old Lootsberg Pass (A) GoogleEarth image of study area on which the measured sections are plotted showing their spatial relationship relative to topography. (B) Twelve measured stratigraphic sections, along with intervals from which independently oriented samples collected mainly as drilled cores were taken for magnetostratigraphy marked with a "P," used to characterize vertical and lateral facies relationships in a magnetostratigraphic context. A composite section of ~240 m thickness is constructed using sections [5], [2], and [3]. Dotted and dashed lines with feathered ends illustrate thick, fine-grained wacke bodies, the bounding surfaces of which are traced physically and used as correlative datums. Star indicates the position of a porcellanite from which Gastaldo et al. (2015) report an Early Changhsingian age in the stratigraphy. GPS coordinates for the Old Lootsberg Pass section, as reported by Ward et al. (2000), corrected for longitude, appear as a solid black dot. GPS coordinates for the base and top of each section are provided in supplemental information. Scale = 0.5 km.**

## STUDY LOCALITY AND METHODS

Fossiliferous stratigraphic sections are located on the Blaauwater 65 and 67 farms, Eastern Cape Province, along the escarpment adjacent to the graded road, as well as railway line, that served as transportation routes over Old Lootsberg Pass (S31°47.771′, E24°47.861′: note all Global Positioning System [GPS] data reported in World Geodetic System [WGS] Datum 84; Fig. 3; Gastaldo et al., 2017). Ward et al. (2000, 2005) report a stratigraphic section for West (Old) Lootsberg Pass at S31°47.600′, E24°47.754′, which is situated within our general geographical coverage (Fig. 3), below the railway line. Outcrop is restricted to exposures in dongas (erosional gulleys) and cliff faces, and along the graded roadway to near the top of the pass where it converges with the railway line (Fig. 3A). Exposure also is present along parts of the railroad cut that transects sandstone of the Katberg Formation. Twelve stratigraphic sections were measured using a leveling Jacob's staff and standard field techniques across a northwest to southeast straight-line distance of >2 km. More than 740 m of stratigraphic section were measured, described at a centimeter-scale resolution where possible, and physically correlated across the area by walking the upper contacts (bounding surfaces) of two major fluvial complexes which provide for true datums in the area (Figs. 3B).

## Geochronologic Methods

Two beds of light-gray (Munsell N8), well-cemented, silty, very fine wacke were discovered during section measurement (S31°48.157′, E024°48.594′ ± 3 m) and sampled for geochronology. These beds supplement, and are distinct from, a well-silicified porcellanite reported by Gastaldo et al. (2015) from the area. The new beds were disaggregated and partitioned into a zircon concentrate by standard rock-crushing and mineral-separation methods, resulting in recovery of an abundant population of zircon grains from the lower bed. Zircon grains were pretreated by chemical abrasion to remove radiation-damaged and altered zones (Mattinson, 2005) by placing them in a muffle furnace at ~1000 °C for ~48 h to restore crystallinity, followed by partial dissolution in 50% HF in Teflon dissolution vessels at 200 °C for ~17 h. Each zircon fragment was cleaned in $HNO_3$, and transferred to a miniaturized Teflon bomb (Krogh, 1973). A mixed $^{205}Pb$-$^{233–235}U$ spike was added to the Teflon dissolution capsules during sample loading (EARTHTIME community tracer, to facilitate inter-laboratory comparisons, see www.earth-time.org). Zircon was dissolved using ~0.10 mL concentrated HF acid and ~0.02 mL 7N $HNO_3$ at 200° C for 5 days, dried to a precipitate, and re-dissolved in ~0.15 mL of 3N HCl. Uranium and lead were isolated from the zircon solutions using anion exchange chromatography, dried down in dilute phosphoric acid, deposited onto out gassed rhenium filaments with silica gel (Gerstenberger and Haase, 1997), and analyzed with a VG354 mass spectrometer using a Daly detector in pulse counting mode. Corrections to the $^{206}Pb$-$^{238}U$ and $^{207}Pb/^{206}Pb$ ages for initial $^{230}Th$ disequilibrium in the zircon data have been made assuming a Th/U ratio in the magma of 4.2. Laboratory procedural blanks are routinely at the 0.5 picogram and 0.1 picogram level for Pb and U, respectively. All common Pb was assigned to procedural Pb blank. Dead time of the counting system for Pb was 16 ns and 14 ns for U. The mass discrimination correction for the Daly detector is constant at 0.05% per atomic mass unit. Amplifier gains and Daly characteristics were monitored using the SRM 982 Pb standard. Thermal mass discrimination correction for Pb is 0.10% per atomic mass unit. U fractionation was measured internally and corrected for each measurement cycle. Decay constants are those of Jaffey et al. (1971), and age calculations were done using an in-house program by D.W. Davis. All age errors quoted in the text and table, and error ellipses in the Concordia diagrams are given at the 95% confidence interval. Plotting and age calculations were done using Isoplot 3.00 (Ludwig, 2003).

## Magnetic Polarity Stratigraphy

For most of our study, samples were collected by drilling oriented cores using a portable field drill with a non-magnetic diamond drill bit. Typically, seven to 12+ independently oriented core samples were obtained from each suitable bed (independent sampling site). Most beds sampled are exposed in the main donga (Fig. 3 [section 5]; WLP01–WLP52; WLP112–WLP120) and adjacent to the Old (West) Lootsberg Pass roadway ([section 6] WLP53–WLP62). A donga section correlative with the roadway was sampled ([section 2] WLP80–WLP102), and the section was extended upwards into the Katberg Formation along another donga section ([section 3] WLP150–WLP161). Sampled lithologies consist of medium- to coarse-grained siltstone and very fine wacke, in addition to several nodular (concretions) horizons in fine siltstone/mudstone (see supplemental data). The number of independently oriented samples obtained is relatively high because of the implicit need to fully characterize the magnetization in the rocks of this succession and to convincingly assess the homogeneity, or lack thereof, of the remanence at each stratigraphic level. This approach differs from all previous studies of presumably uppermost Permian and lowermost Triassic strata in the Karoo Basin where field evidence suggests that only a single independently oriented sample (core) per horizon was obtained (De Kock and Kirschvink, 2004; Ward et al., 2005). In part, full characterization of the remanence is needed because of the extensive suite of mafic (diabase) intrusions of the Early Jurassic Karoo Large Igneous Province that was emplaced throughout the Eastern Cape Province (e.g., Duncan et al., 1997; Jourdan et al., 2005; Svensen et al., 2012). In the Old Lootsberg Pass area, two Karoo intrusions are well-exposed and both of these also were sampled. One intrusion (WLP172) exhibits a sill-like geometry and is <10 m thick. It is exposed ~1.5 km to the south of Blaauwater Farm 65 and, thus, is emplaced into strata over 100 m below our composite section. At this locality, we also sampled host Beaufort Group strata both immediately below (WLP171) and immediately above (WLP173) the mafic sill. The other site (WLP162) was established in a much thicker intrusion, with an overall sill-like geometry that defines the crest of the east-west topographic escarpment that can be traced for 10s of kms above the study area. Near Old (West) Lootsberg Pass, itself, this sill cuts down section to the west and is well-exposed along the railroad siding, some 150 m to the west of our composite section. Most of these intrusions in the Eastern Cape Province, including the two we sampled, are of normal polarity (Hargraves et al., 1997; Geissman and Ferre, 2013). It is necessary to separate an inferred early acquired, normal polarity remanence in upper Permian and inferred lowermost Triassic strata from a normal polarity Early Jurassic "overprint," which is not necessarily straightforward (Lanci et al., 2013; Maré et al., 2014). Published paleomagnetic results from such strata in the central Karoo Basin (Eastern Cape Province) are associated with limited documentation and, thus, confusing. For example, there is no evidence, based on the data reported, that reverse polarity magnetozones exist that are defined by consecutive samples exhibiting well-behaved, stable endpoint magnetizations of reverse polarity in any of the reported sections (De Kock and Kirschvink, 2004; Ward et al., 2005).

Core samples were processed into standard 2.2 cm high specimens for remanence and rock magnetic measurements. Each specimen was washed in dilute HCl to remove any form of metal contamination after specimen preparation. For those stratigraphic intervals lacking beds suitable for drilling, samples were collected as oriented blocks of a range of sizes by marking the orientation of any flat surface of a block that could be removed from the outcrop. Typically five to eight oriented blocks were obtained from a single (<0.5 m) stratigraphic interval. These were re-cut into multiple, 2.0 cm cubical specimens using a non-magnetic diamond saw blade. The nomenclature for our magnetostratigraphic sample collection utilizes a "WLP" prefix (West Lootsberg Pass, synonymous with Old Lootsberg Pass).

Remanence measurements were made on either (1) a 2G Enterprises, DC SQUID, three-axis pulse cooled superconducting rock magnetometer, interfaced with an automated specimen handler, and an online alternating field (AF) degausser system, or (2) JR5A or JR6A AGICO spinner magnetometers. All magnetometers and related demagnetization instrumentation are housed inside a large magnetic shield (Version #50 of Lodestar Magnetics) with an ambient field of less than 300 nT over most volume. In addition, specimens were housed in multilayered mu-metal shields, with ambient fields less than 10 nT, in between thermal demagnetization steps and measurements. Li et al. (2017) demonstrate that the principal magnetic phase in siltstone exposed in the Old (West) Lootsberg Pass section is mainly magnetite, although hematite carries part of the remanence at some sites. Consequently, a subset of specimens prepared from samples from all sites was subjected to both thermal and AF demagnetization. Thermal demagnetization was carried out using one of three ASC TD48, dual zone thermal demagnetizers, in a progressive fashion involving 20–30 steps, sometimes to

maximum laboratory unblocking temperatures of 680 °C (±). AF demagnetization was carried out using the integrated 2G Enterprises AF demagnetization system, typically to peak fields of 90–120 mT.

Acquisition of isothermal remanent magnetization (IRM) and backfield demagnetization of saturation IRM (SIRM) utilized an ASC multicoil impulse magnet system. Three-component thermal demagnetization of IRM acquired in different direct current (DC) fields followed the method of Lowrie (1990). Anisotropy of magnetic susceptibility (AMS) measurements were made using either an AGICO KLY-3S or a MFK1A automated magnetic susceptibility instrument. Measurements of the variation in magnetic susceptibility, as a function of heating and cooling, were carried out on bulk-rock powders or magnetic separates from powders of block samples collected from selected sites using an AGICO CS-4 apparatus interfaced with a MFK1A susceptibility instrument. These measurements were conducted in an argon atmosphere.

Results of progressive demagnetization were inspected using orthogonal demagnetization diagrams (Zijderveld, 1967), and the directions of magnetization components identified by the colinearity of several demagnetization data points determined using principal components analysis (Kirschvink, 1980). Magnetization directions at the site level were estimated as mean directions using as many independent observations as accepted, following the method of Fisher (1953). These estimated site mean-magnetization directions were transformed into virtual geomagnetic poles (VGPs) and plotted on the cumulative stratigraphic column (Opdyke and Channell, 1996) to reveal the magnetic polarity stratigraphy of our section. Estimated paleomagnetic pole positions (e.g., Van der Voo, 1993; Torsvik et al., 2012, Muttoni et al., 2013) for Africa during the late Permian to early Triassic time are such that normal polarity magnetizations in these strata in the Karoo Supergroup in the Eastern Cape Province of South Africa are expected to have a north-northwest (~330°) declination and moderate to steep negative (~60°) inclination magnetization.

## LITHOFACIES

Six principal lithofacies, and variants thereof, are recognized in the Old (West) Lootsberg Pass area (Fig. 3). These are similar to ones reported by us elsewhere and include, from coarsest to finest grained facies: pedogenic nodule conglomerate (Pace et al., 2009); fine to very fine wacke; olive gray and reddish-gray siltstone (Gastaldo et al., 2009, 2014; Pace et al., 2009; Prevec et al., 2010; Li et al., 2017); silicified (porcellanite) siltstone/silty sandstone (Gastaldo et al., 2015); and claystone.

### Pedogenic Nodule Conglomerate

The PNC lithofacies is an intraformational pebble-conglomerate that is matrix supported and composed of small (<0.5–3 cm diameter) calcite-cemented nodules, mudclasts, and bone fragments in a very fine-grained wacke and/or coarse siltstone (Fig. 4). Unweathered rock is pale olive (10Y 6/2) but weathers moderate yellowish brown (10YR 5/4), dusky brown (5YR 2/2), or brownish black (5YR 2/1). Both nodules and matrix are calcite cemented. Nodules range in shape from sub-rounded rods to well-rounded spheres; others are amorphous (Fig. 4A). Sandstones in the lowest part of the stratigraphic section, in which conglomerate lags are found, are traceable over a distance of 3.5 km (Fig. 5); these lags are comprised of intraformational clasts up to 20 cm in length (Figs. 4C, 4D) which exhibit subangular morphologies. Accumulations are concentrated either in channel-lag deposits, ≤1 m in thickness, or as thin (1–3 cm) to medium thick (10–30 cm) lenses with undulatory bases that are in sharp erosional contact within encasing siltstone and/or sandstone. A few lenticular accumulations, found higher in our section, have undergone dissolution and reprecipitation, with dusky brown bodies consisting of sandstone cemented by crystalline calcite (Fig. 4B). Primary sedimentary structures in all deposits vary from planar to low-angle trough-cross or sigmoidal-cross beds (Fig. 4C). Relative to the other lithofacies, the occurrence and distribution of the PNC are rare, and comprise an estimated 0.1% of rock volume or less.

### Fine to Very Fine Wacke

Moderately to poorly sorted, fine- to very fine-grained sand-sized clasts are organized into decimeter-scale massive (Sm; Miall, 1996), planar (Sh), and lenticular beds that grade upwards into thin-to-medium, low-angle (Sl) and trough crossbeds (St; Fig. 6). Ripple lamination

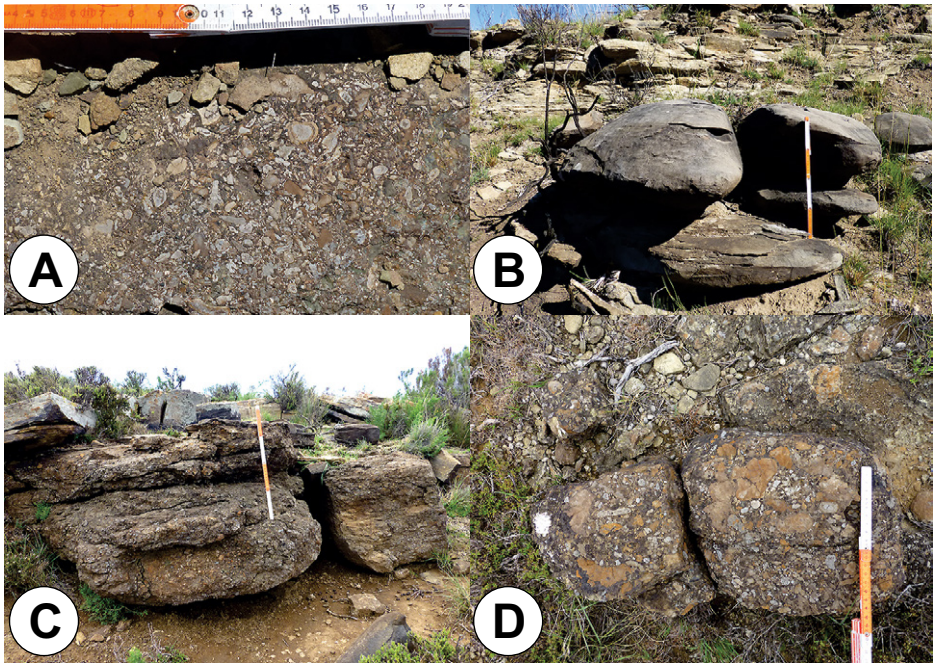


**Figure 4. Coarse-grained lithologies. (A) Exposure of pedogenic nodular conglomerates (PNC) enveloped in reddish-gray siltstone (S31°47.790′, E024°48.345′) in section 11 (see Fig. 3) below the lower datum sandstone. Scale in centimeters. (B) Calcite-cemented, fine to very fine lenticular wacke, weathered brownish gray (5YR 4/1) indicating the presence of recrystallized PNC deposits in fluvial sequences. These appear as lenticular trough fills in lower datum sandstone in section 7. Scale in decimeters. (C) Meter-thick, low-angle, cross-bedded, intraformational pedogenic nodule conglomerate found as a channel-lag deposit at the base of the lowest, thick sandstone body (S –31.823713, E 24.81624; Fig. 5). Scale in decimeters. (D) Intraformational conglomerate outcropping as a pavement exposure (S –31.830796, E 24.823486) in which large reworked clasts are interspersed with calcite-cemented pedogenic nodules, mudclasts, and fragmented bone. Scale in decimeters.**

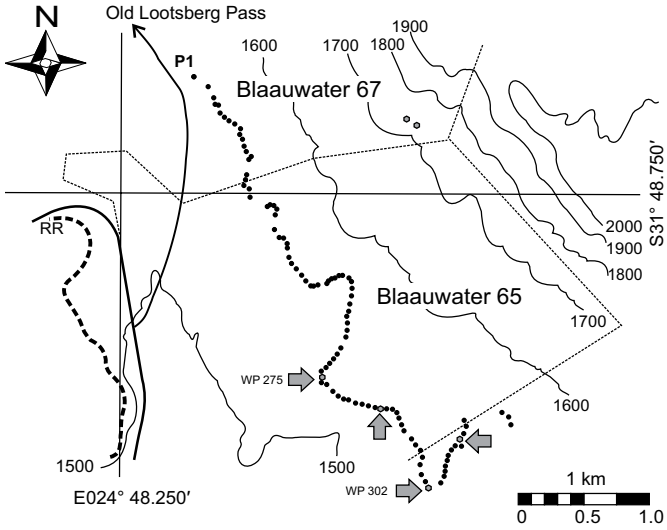


**Figure 5. Map of Blaauwater 65 and 67 farms over which the lowest, thick sandstone body was physically traced. Solid dots mark waypoints taken along the upper contact (bounding surface) along the transect; arrows and gray dots mark the positions (WP—waypoint) of intraformational, pedogenic nodule conglomerate as channel lag deposits (Figs. 4C, 4D). Boring site P1 is provided for reference to other maps. Contour interval is 100 m; scale = 1 km.**

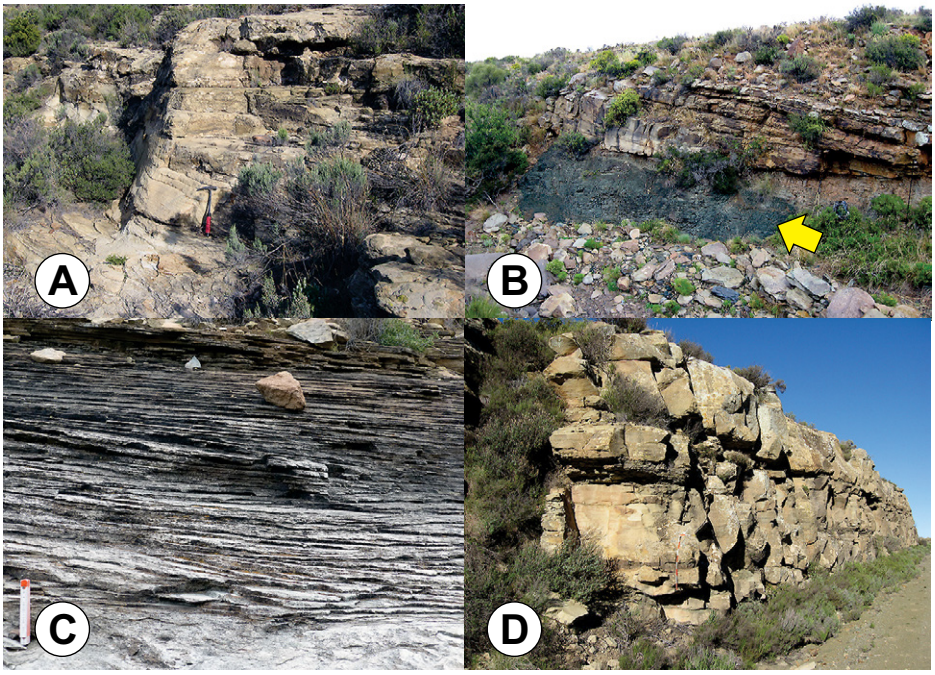


**Figure 6. Sandstone Features. (A) Meter-scale, trough cross-bed sets characteristic of bedload deposits of the fine- to very fine-grained wacke. Image of sandstone body used as the lower correlation datum in Figure 3, marking the base of the Katberg Formation (S31°47.790′, E024°47.813′). Hammer for scale. (B) Part of a lateral accretion barform overlying pedogenically modified coarse siltstone at arrow (S31°47.829′, E024°47.969′) at a stratigraphic height of 75 m. (C) Centimeter- to millimeter-scale, low-angle crossbeds characteristic of upper parts of trough fills. Scale = 10 cm. (D) Thick, multistoried wacke with pedogenic nodular conglomerate–bearing conglomerate lag deposits which may separate individual channel stories, along the Old Lootsberg Pass roadway in the Katberg Formation (S31°47.673′, E024°48.369′).**

(Sr) occurs on laminar bedform surfaces. Small (millimeter-scale), angular mudclasts of coarse-sand size, along with mica flakes and disseminated organics, may be present. The proportion of coarse silt and very fine sand often is difficult to distinguish in the field because of the poor sorting and the massive character of many beds; discrimination between these categories must be via thin section analysis. Often, beds fine upwards resulting in a succession of low angle, millimeter-scale crossbeds that occur as upper parts of trough fills (Fig. 6C). Color ranges from a greenish (5GY 6/1) to yellowish-gray (5Y 7/2), or may be light blue gray (5B 6/1) to medium or light gray (N5–N6); often, the lithofacies weathers grayish orange (5YR 8/4; Fig. 6D). Sandstones are silica cemented, except where lenticular bodies are calcite cemented as noted above, and beds are bounded by upper and lower sharp contacts, the latter often are erosional into underlying siltstone (Fig. 6B). Lower contacts may show evidence of soft-sediment deformation and flow structures.

### Olive Gray Siltstone

Massive or bedded siltstone varies in color, with greenish-gray (10Y 5/2), olive gray (5Y 5/2), and light olive gray (5Y 6/1) common. Grain size also varies from coarse to fine-grained (Figs. 7A, 7B). Depositional cycles generally fine upwards and exhibit sharp lower and upper contacts, although gradational transitions also occur. Calcite-cemented concretions or nodules, brownish-gray (5YR 4/1) in color, may occur within a few meters of the upper contact, and range in size from <10 cm to >1.0 m in length (Fig. 7D). At a few stratigraphic positions, concretionary intervals appear to be amalgamated into a laterally contiguous horizon. Grayish-red (5R 4/2) color mottling may be found in massive intervals (Fig. 7C). Often, siltstones are highly weathered, resulting in a rubbly and blocky appearance, but millimeter-to-centimeter thin-bedded intervals occur spatially isolated in parts of a few measured sections. Where present, olive-gray beds alternate with reddish-gray beds (Figs. 7E and 7F; Li et al., 2017). Several intervals preserve the burrow assigned to *Katbergia*, an indicator taxon of wetland soils (Gastaldo and Rolerson, 2008) or temporally emergent channel barforms (Li et al., 2017).

### Reddish-Gray Siltstone

Generally massive intervals of dark reddish-brown (10R 3/4) to grayish-red (5R 4/2) or brownish-gray (5YR 4/1) siltstone may be either predominantly coarse or fine, and exhibit

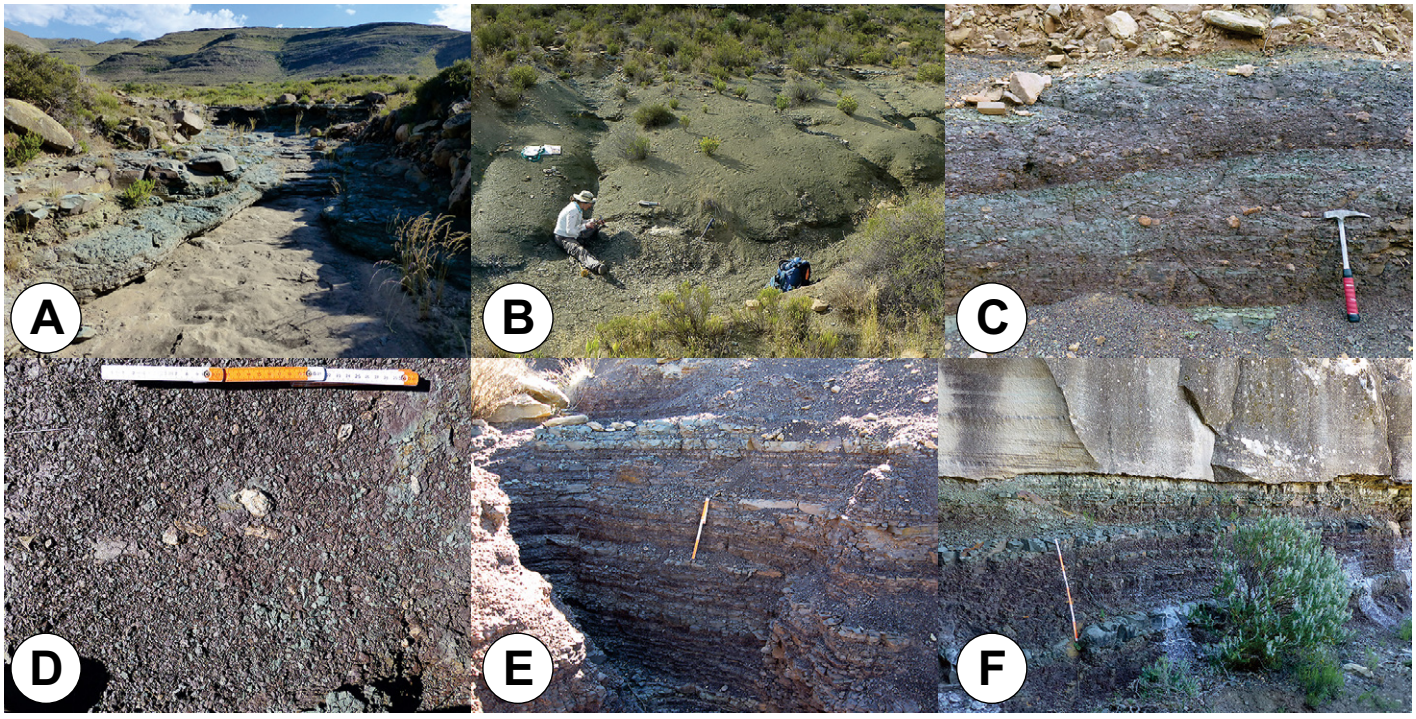


**Figure 7. A color spectrum of fine grained lithologies. (A) Light olive (5Y 6/1) siltstone. (B) Fossiliferous, olive-gray (5Y 4/2) siltstone (Gastaldo et al., 2015). (C) Olive-gray siltstone mottled with reddish-gray (5R 4/2), indicating redox reactivity and color alteration in response to water table fluctuations (see Kraus and Hasiotis, 2006; Li et al., 2017). Hammer for scale. (D) Reddish-gray (5R 4/2) fine siltstone with remnant light olive-gray coloration. Scale in decimeters. (E) Heterolithic, interbedded light olive-gray and reddish-gray, coarse- and fine-siltstone interval, section 10 (Fig. 3), at a correlative stratigraphically position to the lowest datum sandstone body. Scale in decimeters. (F) Heterolithic, interbedded olive-gray and grayish-red, coarse- and fine-siltstone interval, section 6, in the Katberg Formation. Scale in decimeters.**

fining upwards sequences (Fig. 7D). At times, elliptical to lenticular, thin (<0.5 m) bodies of olive-gray or light olive-gray siltstone remain prominent and enveloped in the reddish-gray lithofacies. As above, siltstones are weathered, resulting in a rubbly and blocky appearance, but millimeter-to-centimeter thin-bedded intervals may be encountered. These occur at several stratigraphic levels where cm-scale, olive-gray siltstone alternates with reddish-gray siltstone (Figs. 7E, 7F). Similar to the previous lithofacies, calcite-cemented concretions may be present (Fig. 7A), generally within 0.5 m of the upper facies boundary, with individual sizes ranging from <5 cm to >1 m. Bioturbation includes: inclined, small diameter (centimeter) *Katbergia* burrows; and inclined, large (>20 cm diameter), cylindrical burrows that may extend up to 0.5 m or more in depth and filled with the overlying sediment (very fine wacke or olive-gray siltstone; Gastaldo et al., 2017).

### Silicified (Porcellanite) Siltstone

Beds of silicified siltstone and sandy siltstone are found as part of two channel-fill complexes in the lower 70 m of our stratigraphic section. The basalmost occurrence consists of thin, silicified beds of fine quartz sand-and-silt and volcanigenic clasts in a thin-bedded siltstone interval from which a suite of Early Changhsingian zircons are reported (Fig. 8; Gastaldo et al., 2015). The upper occurrence is ~15 m stratigraphically higher and is part of an overlying fluvial channel system from which a suite of euhedral zircon crystals also has been recovered and analyzed (Fig. 9; see below).

The silicified beds from which Gastaldo et al. (2015) report a Changhsingian maximum age are bluish (5B 9/1) or very light gray (N8) to white (N9; Fig. 8B), and differ in color from the surrounding olive-gray siltstone. Centimeter-scale intervals in the lower part of the succession consist of millimeter- and sub-millimeter scale crossbeds and starved ripples (Fig. 8C), contorted beds, and micro-scale ball-and-pillow structures, which may be accompanied by minimum bioturbation. A population of euhedral, elongate, and pristine zircons comes from a thin (3 cm) unit composed of two, coarse-to-fine silt fining up intervals (Fig. 8D; Gastaldo et al., 2015). Planar opaque laminae occur in the lower part of each fining up succession, which are interpreted as compressed plant debris based on morphological features. No opaque lamina fluoresces when subjected to an ultraviolet source, which is likely a function related to local dolorite intrusions and heating as is the case with recovered palynomorphs (Gastaldo et al., 2017). The fine fraction consists of randomly oriented, elongate euhedral crystals, some of which are subvertical, embedded in a silica matrix without opaque laminae. There is no evidence of sedimentary structures indicative of bedload-sediment transport, as is the case with underlying silicified beds (Fig. 8C). X-ray fluorescence data from five silicified beds in the succession indicate a high percentage of $SiO_2$ (78%–80%), moderate percentages of $Al_2O_3$ (11%) and $Na_2O$ (5%), and low percentages of CaO (1.3%), $K_2O$ (1.3%), and FeO (1%). No geochemical difference in major elemental concentration was found between any well-silicified bed in the interval (Lipshultz et al., 2015).

The stratigraphically higher zircon-bearing siltstones are found as lenticular trough fills in a channel barform (Fig. 9). These thick (5–10 cm) beds are light gray (N8) in color with the lower bed appearing massive. In contrast, the upper bed exhibits millimeter-scale, low-angle primary structures in outcrop. Both units

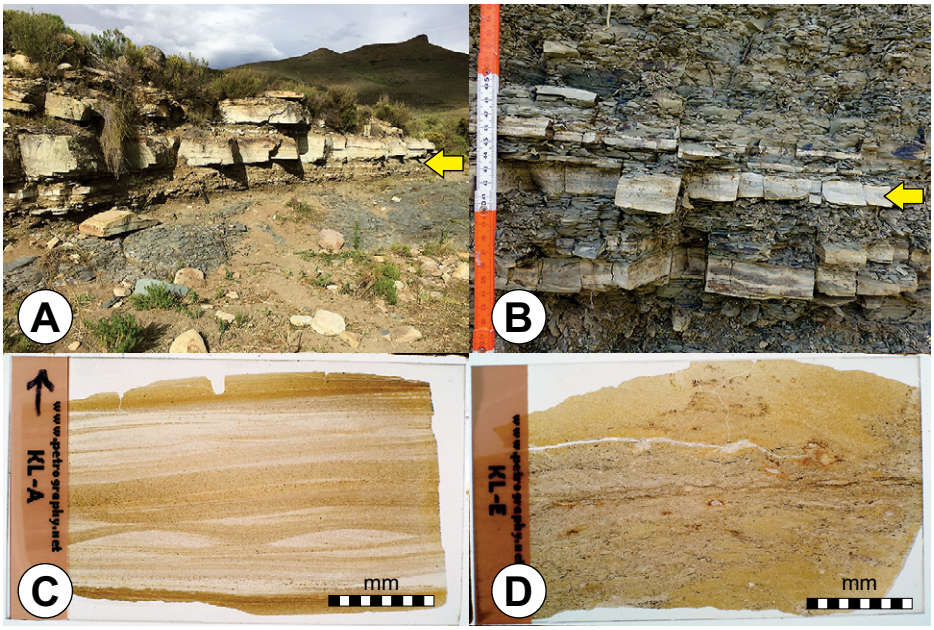


**Figure 8. Channel-fill succession in which a zircon-bearing porcellanite yields a U-Pb ID-TIMS Early Changhsingian age (Gastaldo et al., 2015). (A) Siltstone, claystone, and silicified siltstone (porcellanite) interval beneath imbricated, lenticular fine-grained wacke (S31°48.161′, E024°48.304′). Yellow arrow indicates the position of porcellanite. (B) Light bluish-gray and white, silica-cemented siltstone (porcellanite) beds, intercalated with thinly bedded, weakly cemented siltstone and claystone. Yellow arrow indicates the bed from which euhedral, pristine zircons were recovered and dated by Gastaldo et al. (2015). Scale in centimeters and decimeters. (C) Thin section of lowest silicified porcellanite bed showing sub-millimeter scale primary lamination, starved ripples, and fining up beds. These features characterize all but the upper bed. Scale in millimeters. (D) Thin section of bed from which euhedral zircon grains were recovered, showing a more massive and unorganized texture when compared with all subjacent silicified beds. Scale in millimeters.**

are interbedded with: well-sorted, very fine, light olive-gray silty sandstone that preserve ripples at the upper contacts; a coarse, yellowish-olive siltstone without primary structures; and yellowish-gray, very fine to fine sandstone in which millimeter-scale, low-angle crossbeds are present. In thin section, the lower bed appears massive (Fig. 9B), whereas the upper bed shows evidence of micro–cross-stratification (Fig. 9C). In outcrop, the upper bed exhibits ripples, ball-and-pillow, and flame structures in the uppermost 8 cm. Small (3–4 mm diameter) vertical burrows penetrate the upper surface and are circular in transverse section.

### Claystone

Thin beds of the light gray to olive-gray (5Y 6/1–5Y 5/2) claystone are restricted to channel-fill successions. These are found either overlying some, but not all, bedload deposits or as minor trough fills. Claystone beds range from millimeter- to centimeter-scale in thickness, are planar or lenticular, accompanied by micro–cross-stratification in the latter. This lithofacies is found infrequently and, when present, stand out visually from the siltstones in which they occur.

## STRATIGRAPHIC RELATIONSHIPS

Gastaldo et al. (2015) described and illustrated an ~150 m interval at Old (West) Lootsberg Pass and indicated that additional data exist for successions both below and above their published section. This expanded composite stratigraphy of ~240 m is presented in Figure 10, and constructed using measured sections 5, 2, and 3 (Fig. 3) from which paleomagnetic and rock-magnetic data have been acquired. A short section 12, physically correlated in the field by walking bounding contact surfaces, also is shown from which a maximum geochronometric age estimate is herein presented (see below). Lateral facies relationships are described and illustrated using correlations based on a series of short measured sections (Fig. 11) and observations made on the basal, thick sandstone body traced over a distance of ~4 km (Fig. 5).

### Vertical Facies Relationships

The basal-most succession, exposed in the main donga (erosional gully) section (Fig. 3 [section 5]), is organized into repetitive fining up sequences encompassing ~20 m of thickness. Thin, lenticular or planar beds of very fine wacke are overlain by olive-gray or light olive-gray, coarse-to-fine siltstone intervals (Fig. 7). These are truncated by an erosional contact that marks the base of the lowest, thick sandstone body exposed in the area, which served as the base of the stratigraphy published by Gastaldo et al. (2015).

The lowest, thick sandstone varies in thickness over an exposed distance of ~4 km, from a maximum of >12 m in the main donga and exposures at Tweefontein (see the Data Repository material[1]) (Fig. 1), to <1 m in the southeast where it is covered by soil and can no longer be traced, physically (Fig. 5). No outcrop of this sandstone body exists to the west of the donga where soil covers the landscape. Field observations show that this sandstone body also is characterized by the presence of PNC channel-lag deposits in exposures distant to the main donga (Fig. 5); the presence of PNC is a feature previously reported and, thus, interpreted, to be exclusively characteristic of the Katberg Formation (Ward et al., 2000, 2005; Smith and Botha-Brink, 2014). These newly observed PNC-lag deposits appear at a stratigraphic position ~100 m below what were found to represent the lowest occurrence of the facies in the Lootsberg Pass area (Gastaldo et al., 2015). In the new exposures, channel lags consist of intraformational clasts of paleosol origin, calcite-cemented pedogenic nodules, peds, and vertebrate bone, which are up to 20 cm in maximum dimension, (Fig. 4D; ~19 m in Fig. 10) much larger in overall size than comparable clasts higher in the section . Overlying the succession of stacked, trough crossbedded, bedload deposits is a suite of fining up intervals of predominantly coarse-to-fine olive-gray siltstone similar to other deposits, and an interval of centimeter-scale, planar siltstone in which zircon-bearing porcellanite beds are located (Fig. 8).

[1]GSA Data Repository item 2018119, presents rock-magnetic data including orthogonal progressive demagnetization, isothermal remanent magnetization (IRM) and backfield direct-field demagnetization, progressive alternating field (AF) demagnetization of the natural remanent magnetization (NRM), anhysteretic remanent magnetization (ARM), and isothermal remanent magnetization, bulk susceptibility vs. thermal cycling plots, and transmitted (plane and crossed polars) and reflected light photomicrographs, is available at http://www.geosociety.org/datarepository/2018 or by request to editing@geosociety.org.

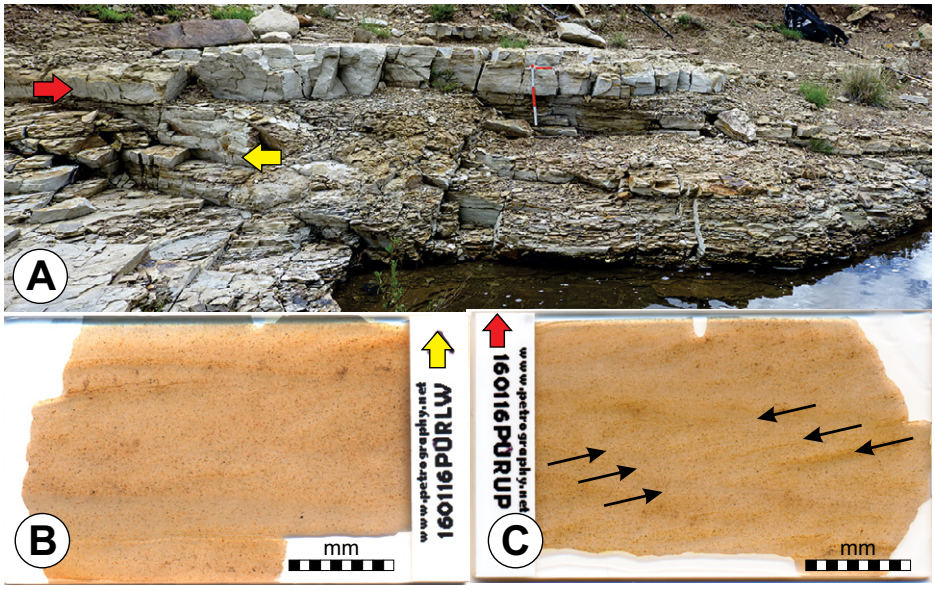


**Figure 9. Cross-bed trough fill of well-silicified, light-gray siltstone from which a suite of zircons yields a Wuchiapingian maximum age for deposition. (A) Outcrop image of erosional gully (donga) exposure showing two well-silicified lenticular beds (at arrows) in less competent sandy siltstone. Scale in decimeters. (B) Thin section of lower bed (yellow arrow) from which euhedral zircon grains were recovered. The bed appears more massive, although faint fining up intervals can be seen. Scale in millimeters. (C) Thin section of upper bed (red arrow) in which micro-crosslamination is preserved. Cross laminae are highlighted by black arrows. Scale in millimeters.**

A 1.1-m-thick interbedded succession of thin-bedded siltstone, porcellanite, and claystone begins at ~42 m in the section (Fig. 10), and is unique in the area. Fining up cycles of silicified siltstone to claystone, on millimeter- and centimeter-scale lamination, characterize much of the interval. Planar, ripple, and micro–cross-stratified beds can be traced across the short exposure (Fig. 8). Lower contacts appear sharp, with most upper contacts gradational except where beds of well-lithified porcellanite occur. Here, lower and upper contacts are sharp as a function of cementation. Centimeter-scale, ball-and-pillow structures of light-gray porcellanite are present higher in the succession, and the upper contact of the highest porcellanite bed is ripple-modified. An en echelon stacked bedset of lenticular wacke overlies these beds which, in turn, is overlain by fining up successions of olive-gray siltstone before encountering a sharp erosional contact with an overlying thick sandstone at ~48 m height. This overlying sandstone body is characterized by low angle, trough cross-bed sets in which a second silicified zircon-bearing siltstone occurs in a correlated lateral exposure (Figs. 9, ~63 m in Fig. 10).

A continuance of the same stratigraphic pattern is replicated vertically over the next ~60 m of section with an increasing light olive-gray siltstone component, the unequivocal presence of a paleosol, truncated erosionally by a point-bar deposit (Fig. 6B; ~72 m in Fig. 10), and the first occurrence in the area of reddish-gray mottling (~77 m in Fig. 10). The paleosol is a coarse, olive-gray siltstone with a maximum exposed thickness of 1.8 m and a granular appearance. Small, vertical rooting structures are accompanied by small, millimeter-diameter (<6 mm) subvertical and subhorizontal cylindrical burrows, which are calcite cemented. Directly overlying the burrowed interval are brown, calcite-cemented, concretions ~70 cm below an erosional contact (Fig. 6B). The overlying barform is 2 m thick and composed of four, lateral accretion, sigmoidal bedforms that can be traced laterally in the donga for >12 m; this outcrop is the only area in which such architectural elements are exposed. A short, 3 m interval of olive-gray siltstone, mottled reddish-gray, occurs above this channel-form deposit (~77–80 m in Fig. 10), and is the first—and only—evidence in the area for color alteration until reddish-gray siltstone is encountered above the datum sandstone of Gastaldo et al. (2015; Li et al., 2017; Fig. 11). Of note is the absence of any 3–5-m-thick interval that can be characterized as either: (1) thinly laminated maroon mudrock of dark reddish-brown and olive-gray siltstone-mudstone couplets (Smith and Ward, 2001, p. 1148); or (2) distinctive thickly laminated reddish-brown siltstone-mudstone couplets, each 1–3 cm thick (Smith and Botha-Brink, 2014, p. 103) in the subsequent succession wherein the Permian–Triassic boundary is purported to occur based on vertebrate biostratigraphy (Fig. 10; Gastaldo et al., 2015, 2017). Olive-gray siltstone continues higher in the stratigraphy until interrupted by an erosional contact with a fossiliferous sandstone in which additional PNC-bearing channel-lag deposits occur (~117 m in Fig. 10). Gastaldo et al. (2015) used this traceable sandstone body as one of several correlation datums across the area (Figs. 3, 11).

Channel deposits in the datum sandstone of Gastaldo et al. (2015) attain a maximum thickness of 12 m and consist of meter-scale, trough crossbed sets that fine upward and exhibit similar characteristics to subjacent sandstone architectures and distribution of primary structures. Thick, meter-scale crossbedded lenses of intraformational PNC are not contiguous across the area but occur sporadically at the base of the system (e.g., sections 2, 7, 8, 11; Fig. 11), and lenses of recrystallized PNC that appear as calcite-cemented trough fills occur higher in the sandstone body (i.e., section 7; Figs. 4B, 11). This sandstone body can be traced over a distance >0.5 km from west to east. The channel deposits thin and pinch out in both directions (Figs. 3, 11) into either olive-gray (west) or reddish-gray (east) siltstone, which dictate the characteristic features of the overlying stratigraphy in these areas.

Lithofacies that overlie the upper datum sandstone in the west, where the composite stratigraphic section is presented, consist of fining up intervals of very fine wacke to olive-gray fine siltstone in which both megaflora and vertebrate remains are preserved (Gastaldo et al., 2015, 2017; 130 m and ~143–146 m in Fig. 10). These olive-gray facies continue for ~25 m whereupon the first evidence of reddish-gray siltstone in the section is encountered (~155 m in Fig. 10; Fig. 11). An erosional contact with a light bluish-gray wacke, over which a thin, intraformational PNC is encountered in a lenticular yellow-gray wacke, outcrops just below the railroad cut (Fig. 3; ~162 m in Fig. 10). Stratigraphically above these sandstones is a short, <0.5 m unit of thin, interbedded olive-gray and reddish-gray planar siltstone beds, the first evidence of a lithofacies similar to what is purported to represent the PTB in the locality (Fig. 11, section 2;Ward et al., 2000). Over the next 65 m of section, coarse-and-fine siltstone intervals, some with *Katbergia* and vertebrate burrows, are colored either light olive-gray, olive-gray, or reddish-gray. Here, the proportion of olive-gray to reddish-gray rocks is 60:40. Higher in the section, at ~218 m, is the occurrence of another light bluish-gray wacke consisting of meter-

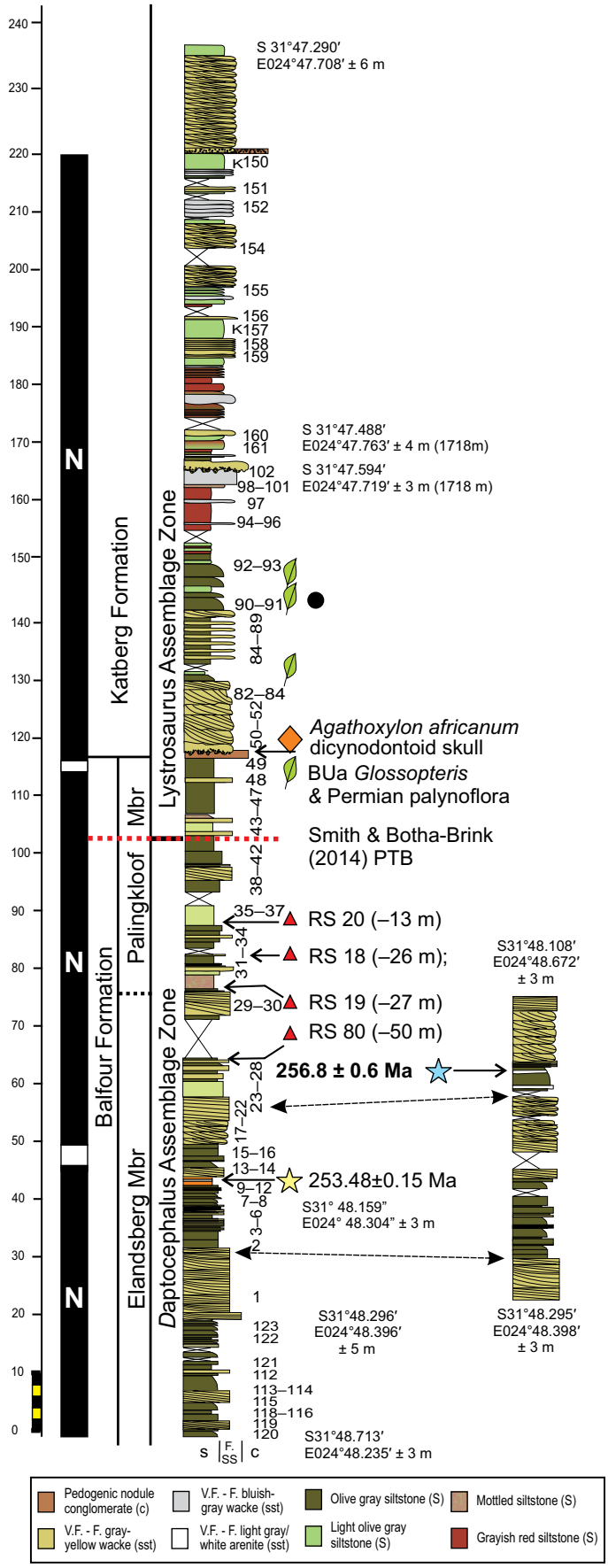


**Figure 10. Long composite stratigraphic section using measured sections 5, 2, and 3 (see: Fig. 3), from which there are a complementary set of borings for magnetostratigraphy, marked as numbers along right side. GPS coordinates are provided for the base and top of each transect, along with its elevation as determined using a Garmin GPSMap 62S unit with barometric altimeter. Yellow star marks the stratigraphic position of a U-Pb ID-TIMS Early Changhsingian age reported by Gastaldo et al., (2015) for the porcellanite interval in orange (Fig. 5). Red triangles mark the stratigraphic position of vertebrates used by Smith and Botha-Brink (2014) and others to circumscribe the *Daptocephalus/Lystrosaurus* biozone boundary in the area (dotted red line; for a discussion on its utility, see Gastaldo et al., 2017). Orange diamond marks the position of permineralized wood and a Permian-aspect dicynodontoid skull reported from the lowest datum sandstone traced in the area (Gastaldo et al., 2015, 2017; Fig. 3). Green leaves mark the position at which *Glossopteris* is preserved in the Katberg Formation. Solid black circle marks the position of the base of the section by Ward et al. (2000) for their Permian–Triassic boundary section based on published GPS coordinates. A short stratigraphic section, physically correlated in the field is shown and marked as section 12 on Figure 3. The stratigraphic position from which a Wuchiapingian age estimate is reported, herein, is marked by a blue star. Inferred magnetic polarity stratigraphic zonation is shown on the left, with normal polarity (N) magnetozones in black, and reverse polarity magnetozones in white. S—siltstone; F. SS—very fine and fine sandstone; C—intraformational conglomerate; sst—sandstone. Scale in decameters.**

scale, trough crossbed sets. The composite section ends in a thick, yellow-gray, crossbedded wacke wherein a ~0.5 m thick, intraformational PNC is present at its base.

### Lateral Facies Relationships

Correlation of measured sections is facilitated by the presence of resistant sandstone bodies along the mountain flanks in areas of steeper topography (Fig. 3). The PNC-bearing sandstone body at a stratigraphic position of ~117 m is used as one traceable datum (Fig. 10) at Old (West) Lootsberg Pass, with bounding surfaces associated with higher sandstones supplement-

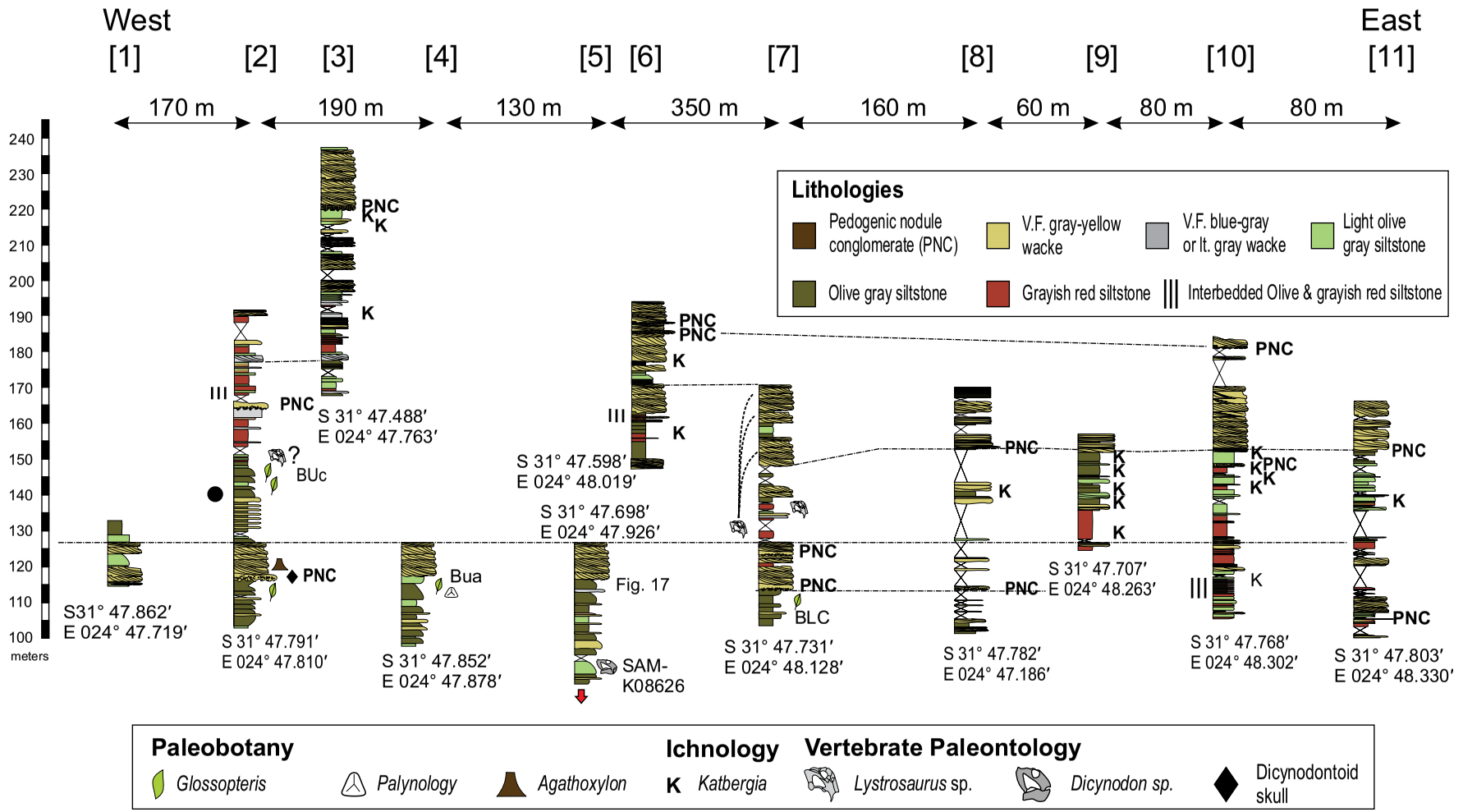


**Figure 11. Correlation of eleven measured sections across an ~800 m distance using the thick, multistoried sandstone datum (see Figs. 3, 10) at the base of the Katberg Formation. Note the occurrence of interbedded olive-gray and reddish-gray siltstone intervals (vertical, parallel lines), considered by other workers (Smith and Ward, 2001; Ward et al., 2005; Smith and Botha-Brink, 2014) as a unique, and mappable marker bed heralding the end-Permian terrestrial extinction event. Siltstone coloration is markedly different in correlative beds in a west-to-east direction, changing from olive-gray and light olive-gray to reddish-gray (see Li et al., 2017). Dashed and dotted lines indicate correlative upper contacts (bounding surfaces) of bedload deposits traced, physically, across the area. Solid black circle marks the position of the base of the section by Ward et al. (2000) for their Permian–Triassic boundary section based on published GPS coordinates. *Glossopteris*-bearing horizons reported by Gastaldo et al. (2015) include BUa, BUc, and BLC. K—preservation of *Katbergia* ichnogenus.**

ing correlation between 11 measured sections (Fig. 11). Siltstone exposed below the datum in all but sections 9 and 11 is consistently of either light olive-gray or olive-gray color. The exception is a thin unit of reddish-gray siltstone in the easternmost section (section 11; Fig. 10) in which an isolated lens of PNC occurs (S 31°47.790′, E024°48.345′). Siltstone intervals in the datum sandstone at ~117 m may be either light olive-gray (section 1) or reddish-gray (section 7) with laterally correlative units of an interbedded olive-gray and reddish-gray character toward the east, and the presence of *Katbergia*-burrowed units terminating the succession (section 10; Fig. 11). The same spatial trend in siltstone color is found higher in the section.

Fining up sequences of wacke overlain by olive-gray siltstone characterize the westernmost fine-grained lithologies. These beds are fossiliferous (section 2; Fig. 11), preserving *Glossopteris* leaves and an articulated, post cranial lystrosaurid skeleton (Gastaldo et al., 2015; 2017). Siltstone color changes eastward to reddish-gray in which an isolated canine of *Lystrosaurus* cf. *murrayi* (section 7; Fig. 11; Gastaldo et al., 2015, 2017) is preserved. The proportion of siltstone in which the color is altered to reddish-gray increases eastward above the datum, along with an increasing presence of *Katbergia*-burrowed paleosols (sections 9–11; Fig. 11). But, reddish-gray siltstone becomes less common in this area beneath the next, stratigraphically higher and traceable sandstone body (sections 7–11; Fig. 11), whereas there is an increasing proportion of reddish-gray siltstone in beds correlative to the west (section 2; Fig. 11). Another grayish-yellow, fine to very fine wacke overlies these siltstone intervals and can be traced over a lateral distance of >800 m where the sandstone body pinches out.

Correlative exposures to the east differ only in siltstone coloration and degree of bioturbation (Fig. 11). Reddish-gray, coarse-to-fine siltstone of varying thickness directly overlies the datum sandstone of Gastaldo et al. (2015). These intervals appear massive in outcrop, but may exhibit millimeter-scale lamination or homogenization in thin section, and extend upwards for ~15 m (Li et al., 2017). Thereafter, fining up successions of either fine wacke to siltstone or coarse-to-fine siltstone occur, but all are either of an olive-gray or light olive-gray coloration with little or no evidence of reddish-gray mottling. Both reddish-gray and olive-gray siltstone are bioturbated by *Katbergia* burrows (Fig. 11, sections 8–11), and the interval is overlain by an erosional contact with a thick, yellowish-gray sandstone, exhibiting the same lithofacies and architectural elements of channel deposits lower in the section. This erosional contact is traced laterally for >1 km and serves as a second correlation datum in this area (Figs. 3, 11).

An erosional contact separates the base of the upper sandstone, herein reported, from underlying fine or coarse siltstone of either light olive-gray or olive-gray coloration (sections 7–11; Fig. 11). The base of that erosional surface incises deeper into underlying rocks in the west than in the east. Intraformational PNC occurs either as thin lenticular beds enveloped in subjacent siltstone or as basal channel-lag deposits at the base of, or in, the lithic wacke body. The sandstone exhibits trough crossbed sets with thicknesses and primary structures of the same character and variability as seen in sandstone bodies found both lower and higher in the area (Figs. 6D, 10). Internally, erosional contacts, which may or may not be overlain by PNC lag deposits, mark the bounding surfaces of architectural elements. Individual stories attain a maximum thickness of ~10 m, whereas amalgamated channels reach >18 m in total thickness. Trough fills range from coarse to fine, olive-gray and light olive-gray siltstone. Reddish-gray mottling of olive-colored siltstone is common. Underlying this multistoried sandstone in the west (section 6) and in a correlative position to it in the southwest (section 2; Fig. 11), are thin, <0.5 m thick intervals of interbedded, or laminated, olive-gray and reddish-gray siltstone. These intervals are similar to what is reported by Ward et al. (2000, 2005) and Smith and Botha-Brink (2014) as the unique facies, characteristic of the PTB in the area. The laminated interval in section 2 is positioned stratigraphically above the GPS coordinates published by Ward et al. (2000, 2005) for their measured section at Old (West) Lootsberg Pass (Fig. 3).

## MAGNETIC POLARITY STRATIGRAPHY AND ROCK MAGNETISM

The intensities of the natural remanent magnetization (NRM) in the sedimentary rocks sampled in the Old (West) Lootsberg Pass section typically range from ~10 mA/m to 0.5 mA/m, with most of the established sites having NRM values less than 5 mA/m. Declinations of NRM directions are largely clustered in the northwest quadrant and inclinations are typically of moderate to steep negative inclination. In progressive demagnetization, specimens from most samples from all sites collected reveal a first removed, well-defined (maximum angular deviation values for unanchored lines typically less than 5°) remanence of northwest to north-northwest declination and moderate to steep negative inclination, thus of normal polarity (Fig. 12). This magnetization component is comparable in direction to the present day field for the Eastern Cape Province, of ~334.7° and –64.8° (World Magnetic Model, 2010). This remanence is also, as noted above, comparable in direction to that of the normal polarity characteristic remanent magnetization (ChRM) of mafic intrusions of the Early Jurassic (ca. 184 Ma) Karoo Large Igneous Province (Hargraves et al., 1997; Geissman and Ferre, 2013). In the southern part of the Karoo Basin, these Karoo intrusions (sills, dikes, and more irregular geometry bodies) are predominantly of normal polarity.

This magnetization component, for most but not all sites, is the principal magnetization component isolated in demagnetization, and is unblocked over a range of laboratory unblocking temperatures to ~580° C and at least 80 percent randomized in alternating field (AF) demagnetization by 80–100 mT (Fig. 12). Specimens from some sites require thermal demagnetization to ~680° C to fully unblock this magnetization. At the site (=bed) level, the between-sample consistency in demagnetization behavior is very high (Fig. DR1, see footnote 1), and the between-sample dispersion is typically very low (Fig. DR1, supplemental material [see footnote 1]), with $\alpha_{95}$ values consistently less than 10°, and precision parameter estimates ($k$) above 75 for sample populations of at least seven independent samples. The typical maximum laboratory unblocking temperatures of ~580° C and median destructive fields of 20–40 mT are consistent with a low-titanium magnetite as the principal carrier of the remanence in these rocks.

The two Karoo intrusions sampled in the Old (West) Lootsberg Pass area (WLP162 and WLP172) both respond favorably to progressive demagnetization and yield well-grouped ChRMs of north-northwest declination and moderate to steep negative inclination (normal polarity; Fig. DR2, supplemental material [see footnote 1]). The Beaufort Group strata sampled at sites below (WLP171) and above (WLP173) the WLP172 site in the mafic sill both yield, in progressive thermal and AF demagnetization, well defined ChRMs with directions that are statistically indistinguishable from the sill (WLP172). The NRM intensities of the host sedimentary rocks both above and below this sill range between 10 and 20 mA/m, and are notably higher than those from rocks sampled in our composite Old (West) Lootsberg Pass section.

With the exception of two narrow stratigraphic intervals, one centered around site WLP17 (and correlative to adjacent "resampled" sites WLP103/104 and WLP170), and the other centered around WLP51 (and correlative to adjacent sites WLP168), all sites that have been studied in sufficient detail show that a

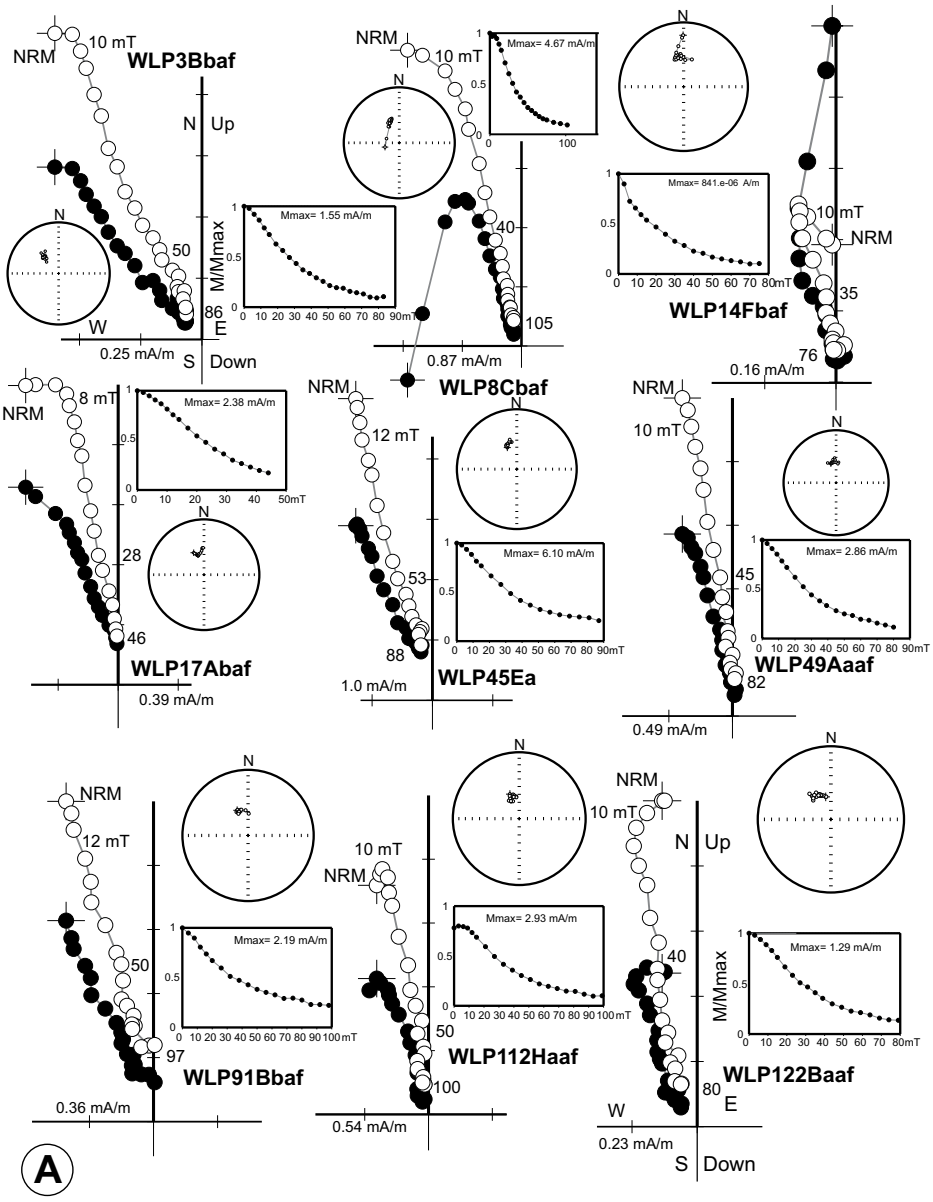


**Figure 12 (*on this and following three pages*). Examples of orthogonal progressive demagnetization diagrams showing the end point of the magnetization vector plotted onto the horizontal (filled symbols) and vertical (open symbols) planes (NS-EW, EW-Up/Down) for individual specimens from samples from selected sites sampled in the West Lootsberg Pass section that have been subjected to progressive alternating field (AF; A) or thermal demagnetization (parts B, C, D). Demagnetization steps, in peak alternating fields (in milliTesla, mT) or temperatures (°C) are given alongside selected vertical projection data points. Also shown are normalized intensity-decay plots showing response to progressive thermal or AF treatment (abscissa is peak temperature, in °C, or alternating field, in milliTesla) and equal area stereographic projections of the magnetization vector measured at each step. Note that the coordinate (geographic) axes for each and every diagram are identical in orientation. NRM—natural remanent magnetization.**

normal polarity magnetization is the principal and only well-defined component of the NRM. For site WLP17 (and 103/104 and 170), specimens consistently show the unblocking of a normal polarity magnetization over a range of temperatures up to between ~400° and 450° C (Fig. 13). Thereupon, specimens reveal the consistent isolation of a remanence of south-southeast declination and moderate to steep positive inclination (therefore of reverse polarity; Fig. 13). The isolation of this reverse polarity remanence is not as well defined (higher maximum angular deviation values for lines anchored to the origin) than that of the normal polarity remanence, in part because the reverse polarity remanence has an intensity that is ~25 percent of the NRM. At site WLP51 (and correlative site WLP168) a similar behavior is observed, but the resolution of a south-southeast declination and moderate to steep positive inclination remanence is less well-defined (Fig. 14). Nonetheless, the specimens from samples from this interval do show the first-removal of a normal polarity remanence, and then the presence of positive inclination data points attending an increase in remanence intensity. Finally, a few additional sites, to date, reveal a consistent hint of the presence of a magnetization that is south-southeast directed and of moderate positive inclination "buried" beneath the normal polarity remanence. This magnetization, if real, is often a small percentage of the NRM and is typically poorly defined. Overall, the Old (West) Lootsberg Pass composite section we have examined is dominated by normal polarity remanence as the principal, well-defined component of the NRM. Thus, the magnetic polarity stratigraphy for this section is characterized by the prevalence of normal polarity magnetozones. The implications of this interpreted polarity stratigraphy are discussed below.

Curves showing the acquisition of an IRM to saturation and backfield demagnetization of SIRM (Fig. DR3, supplemental material [see footnote 1]) are consistent with the interpretation on the basis of progressive demagnetization experiments that magnetite is the principal magnetic phase in Beaufort Group strata. Specimens are fully or nearly fully saturated in fields of ~200 mT, and they yield coercivities of remanence of ~40–50 mT. The overall form of the acquisition curves and the coercivity of remanence values are consistent with a population of magnetite grains dominated by pseudo-single domain sizes. Comparing the response to progressive AF demagnetization of the NRM, anhysteretic remanent magnetization (ARM; peak AF field of 100 mT, biasing DC field of 0.1 mT), and IRM (peak DC field of 100 mT; Fig. DR4, supplemental material [see footnote 1]) further shows that fine, pseudo-single domain magnetite is the dominant magnetic particle component in these rocks. Transmitted and reflected light examination of polished thin sections of samples from selected sites reveals the presence of albeit rare, fine (<<50 micron diameter)

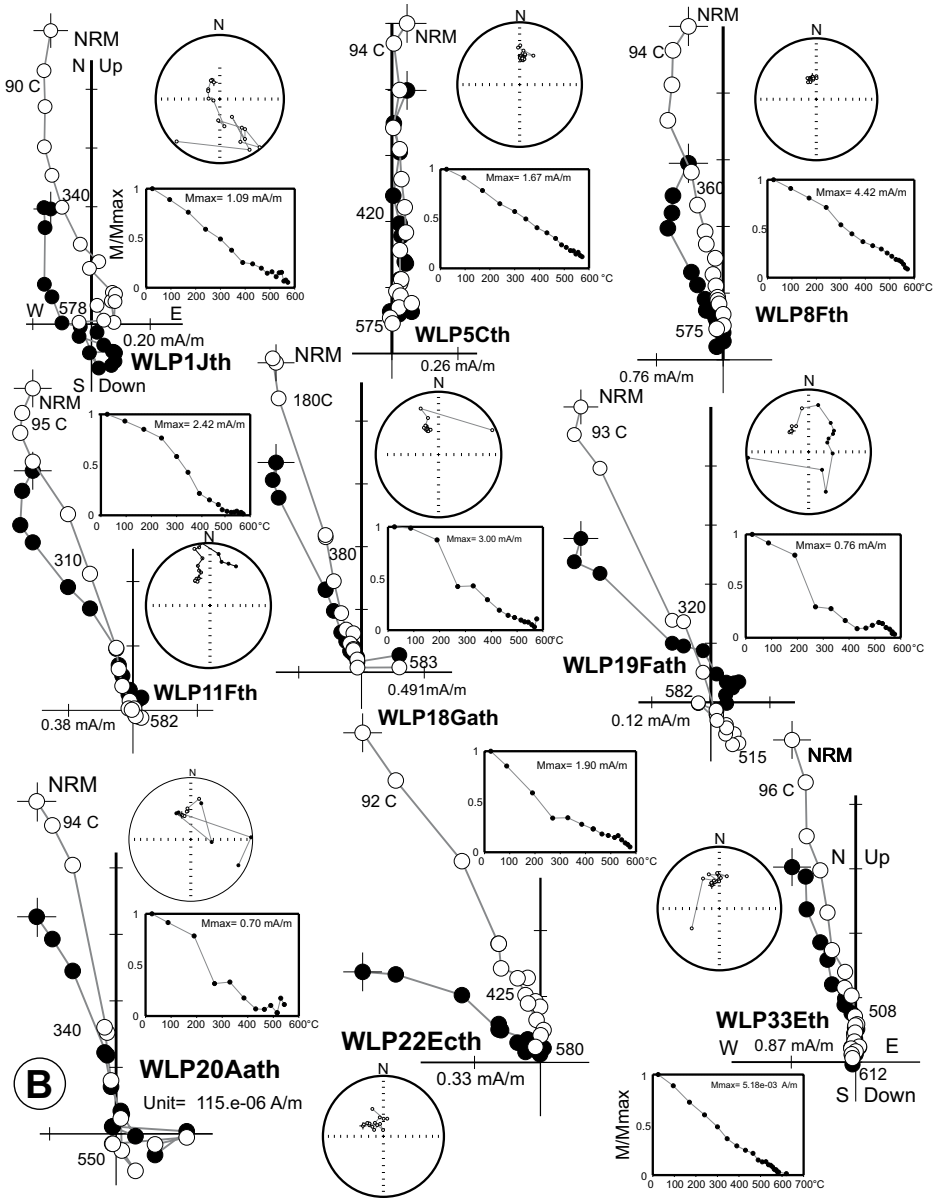


**Figure 12 (*continued*).**

subrounded to rounded magnetite grains that are somewhat smaller in size to most quartz and feldspar detritus (Fig. DR5, supplemental material [see footnote 1]). In reflected light, most magnetite grains are visibly unoxidized. The lack of abundant, obvious detrital magnetite grains having sizes comparable to the somewhat courser silicate detritus is consistent with the relatively low NRM intensities of these rocks and their rock magnetic behavior.

Magnetic separates from large (~0.5 kg+) samples from selected sites require careful preparation. The largest mass magnetic separates we obtained (e.g., site WLP13) all show a significant decrease in susceptibility over a narrow temperature range below ~580° C, indicating nearly pure magnetite as the principal magnetic phase (Fig. DR6, supplemental material [see footnote 1]). Heating curves show a slight Hopkinson effect, demonstrating the presence of at least some multidomain magnetite. The initial heating and cooling curves are close to reversible. Subsequent heating/cooling cycles demonstrate the reversibility of the curves.

## MAGNETIC SUSCEPTIBILITY AND MAGNETIC ANISOTROPY DATA

We collected bulk magnetic susceptibility and anisotropy of magnetic susceptibility (AMS) data from all specimens of appropriate dimension and shape prepared from all samples from most sites in this study (Table 1, supplemental material). AMS data for almost all of the sites sampled as part of the Old (West) Lootsberg Pass composite section are consistent with the preservation of a primary depositional fabric (Fig. 15), as a well-developed oblate fabric. In these cases, minimum susceptibility (Kmin) axes are oriented close to vertical, and Kmax/Kint axes are either relatively well-grouped with subhorizontal orientations or they are uniformly distributed in a subhorizontal plane. The exception is with the few sites established in concretions, where the AMS fabric is very poorly defined (e.g., site WLP107, Fig. 15A). At the site level, the degree of anisotropy (P) ranges from 1.002 to 1.050, with most sites having P values between ~1.020 and 1.030.

We have compiled bulk magnetic susceptibility, remanence, and magnetic anisotropy parameter data from most sites established for this study as a function of stratigraphic position in the Old (West) Lootsberg Pass composite section to examine whether any magnetic properties of these rocks reveal substantial changes that might reflect the previously inferred dramatic modifications to the ecological landscape and ecosystem perturbation associated with the terrestrial End Permian crisis (e.g., Ward et al., 2000; Benton and Newell, 2014; Smith and Botha-Brink, 2014). Plots of bulk MS, NRM intensity, anisotropy T parameter and anisotropy P parameter (Fig. 16) show no distinct changes over a stratigraphic interval between ~110 and 130 m, where we would anticipate the most substantial changes in rock magnetic properties in response to landscape changes. We do note that the dispersion in the mean T parameter (an anisotropy shape parameter, where a value of +1 is associated with a strongly oblate fabric) does increase higher in the section. Correspondingly, the mean P parameter (where P = Kmax/Kmin) shows a slight decrease. At present we consider these variants to be of uncertain significance.

## GEOCHRONOLOGY

The suite of zircon grains isolated from the silicified-wacke trough fill (Fig. 9) exhibits a range of shapes, color, and degree of mechanical abrasion indicating their detrital nature. The lithology is situated ~15 m above the channel-fill from which an early Changhsingian age is reported (Figs. 3, 10, ~44 m; Gastaldo et al., 2015), and is part of an overlying channel complex (Fig. 10, 63 m). U-Pb ID-TIMS analyses of chemically abraded, euhedral zircon grains, in which four concordant results were determined,

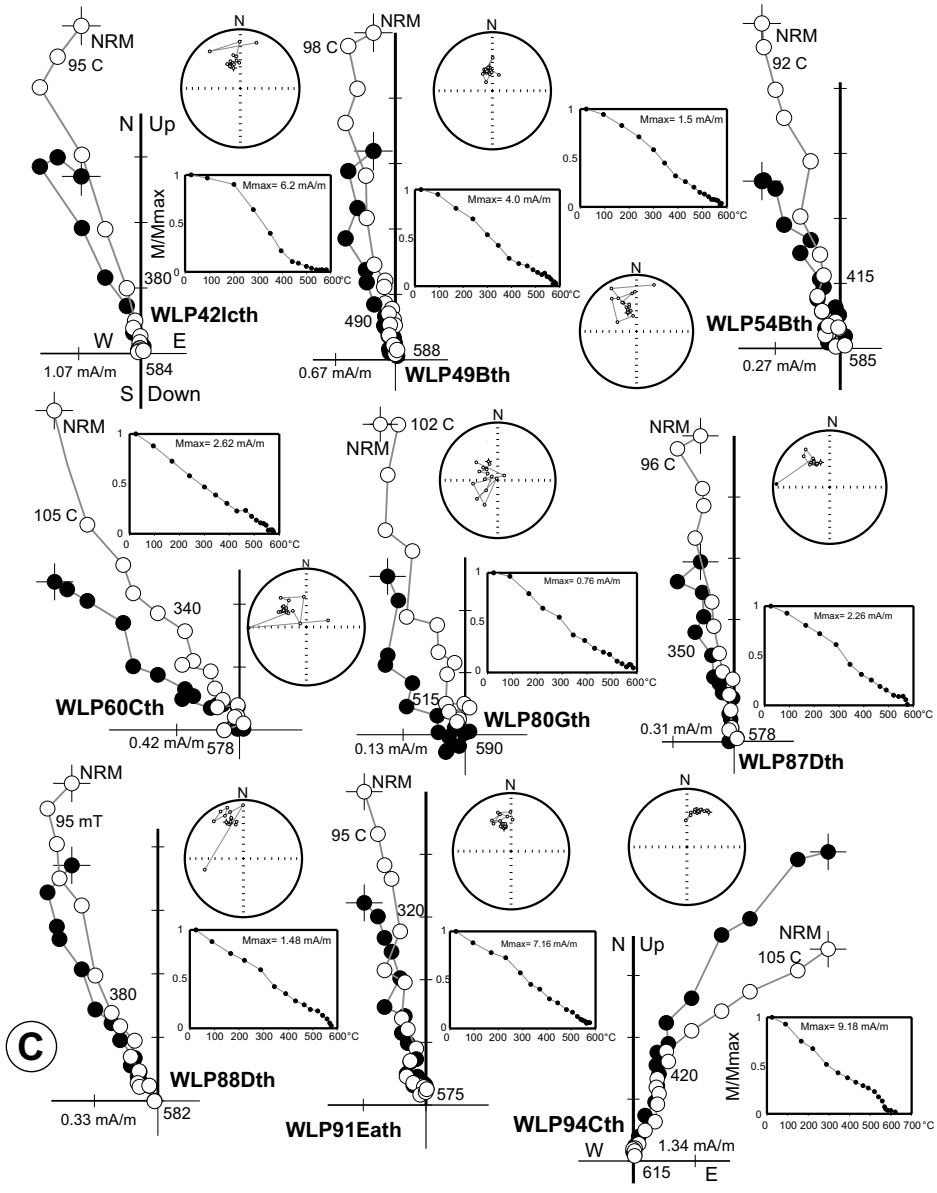


**Figure 12 (*continued*).**

yield a maximum $^{206}Pb/^{238}U$ age for the time of deposition of 256.8 ± 0.6 Ma, the youngest concordant grain (Fig. 17). Hence, the maximum age of this deposit is early Wuchiapingian. And, although the stratigraphic position of the bed is above that from which the Changhsingian age estimate originates, it is older than that of the maximum age from that silicified (porcellanite) siltstone (Figs. 8, 9).

## DISCUSSION

Vertebrate biostratigraphy continues to play the critical role in defining the ecological conditions associated with the reported Permian–Triassic event in the Karoo Basin (Smith, 1995; Smith and Ward, 2001; Ward et al., 2005; Smith and Botha-Brink, 2014; Roopnarine and Angielczyk, 2015; Rubidge et al., 2016; Fig. 2) and also extrapolating that systemic boundary in latest Permian terrestrial strata to other continents (Benton and Newell, 2014; although see Lucas, 2017a, 2017b). The *Daptocephalus* Assemblage Zone (AZ) encompasses most of the upper Permian Balfour Formation (Fig. 2) and is considered to terminate with the reported extinction, or last appearance datum (LAD), of *Daptocephalus* exactly at the assemblage-zone boundary (Viglietti et al., 2016). Currently, this criterion also is considered to represent an end-Permian mass extinction event, placed in the Palingkloof Member of the Beaufort Formation (Ward et al., 2005; Smith and Botha-Brink, 2014; Viglietti et al., 2016; Rubidge et al., 2016, and others). Two species of *Lystrosaurus*—*L. maccaigi* and *L. curvatus*—are reported to have their first appearance datum (FAD) high in the *Daptocephalus* AZ (although see Gastaldo et al., 2017, about discrepancies as to where *Lystrosaurus* is reported to first occur) and their co-occurrence with *Daptocephalus* are considered characteristic of the latest Changhsingian (Botha and Smith, 2007; Smith and Botha-Brink, 2014; Viglietti et al., 2016). Less than 5 m stratigraphically above the assemblage-zone boundary, the FAD of two taxa—*Lystrosaurus murrayi* and *L. declivis*—are reported to be diagnostic of the lowest Triassic rocks (upper Palingkloof Member and Katberg Formation; Botha and Smith, 2007; Lucas, 2010; Smith and Botha-Brink, 2014; Viglietti et al., 2016).

Several lines of evidence are used to place our succession in the upper *Daptocephalus* and lower *Lystrosaurus* AZs. The first is the presence of vertebrates with affinities to either *Dicynodon*, *Daptocephalus*, *Dinanomodon* or *Lystrosaurus* in the PNC-lag deposit of the datum sandstone in the rocks below ~118 m in our section (Fig. 10; Gastaldo et al., 2015, 2017) and a skull of *Daptocephalus*, exhibiting a mixture of anatomical features with *Dicynodon*, within ~35 m of this horizon in a correlative section at Tweefontein (see footnote 1) (Fig. 1; Gastaldo et al., 2017). Their presence supports placement of this part of the stratigraphy in the uppermost *Daptocephalus* AZ. The second are the occurrences of *Lystrosaurus* in rocks above this horizon. The preservation of a *Lystrosaurus* sp. mandible in a gray-red siltstone directly overlying our sandstone datum (Fig. 11, upper bounding surface at ~128 m; *Lystrosaurus* mandible in section 7) does not permit a biozone assignment. However, the presence of *L. murrayi*, in a block of displaced sandstone above the datum, along with two specimens assigned to *L. murrayi* and *L. declivis* (Smith and Botha-Brink, 2014) at the top of our roadway section (Fig. 3 [section 6]), indicate their origin in strata that other authors assign to the Early Triassic *Lystrosaurus* AZ (Botha and Smith, 2007; Fig. 9, 10). Hence, the lithostratigraphic framework described herein transitions the uppermost *Daptocephalus* and lowermost *Lystrosaurus* AZs, as currently defined. Our studied section encompasses the vertebrate-defined, Permian–Triassic extinction event, as currently envisioned (Ward et al., 2005; Smith and Botha-Brink, 2014; Viglietti et al., 2016, 2018; Rubidge et al., 2016), although Gastaldo et al. (2017) present data and a biostratigraphic analysis that casts serious doubt on the stratigraphic position of the assemblage-zone boundary, if one exists at all.

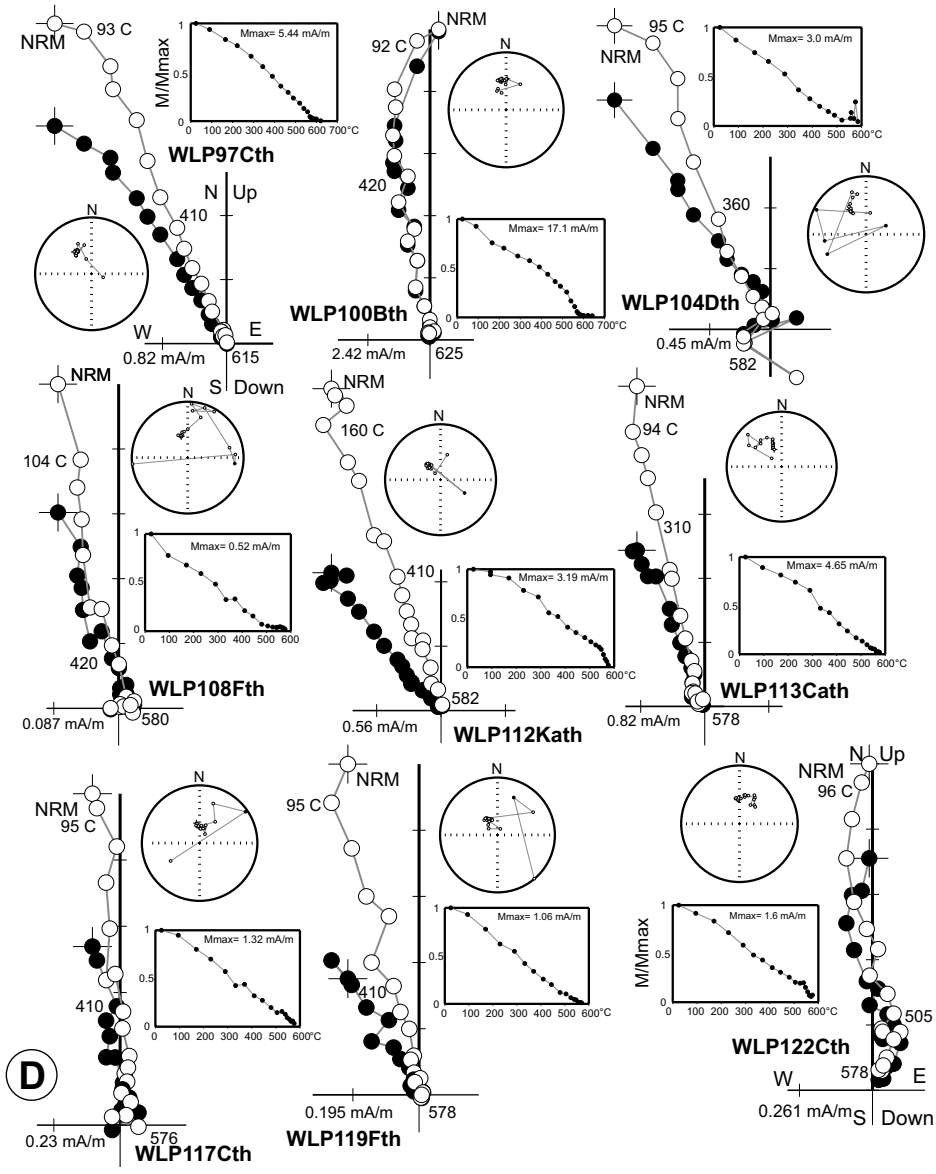


**Figure 12 (*continued*).**

The model for the demise and rapid recovery of these terrestrial ecosystems, which is believed to be coeval with the end-Permian marine event, invokes landscape aridification as a consequence of increased dry monsoonal seasonality. Aridification proxies include an increased proportion of maroon (reddish-gray) siltstone, interpreted as loess deposits and, thus, eolian in origin (Smith and Botha-Brink, 2014; for an alternative explanation see Li et al., 2017), a changeover in fluvial architectural elements, and the appearance of intraformational conglomerate consisting of mudchips, bone fragments, and calcite-cemented pedogenic glaebules and pisoliths (Smith, 1995; Ward et al., 2000, 2005; Smith and Botha-Brink, 2014). Initially characterized in the literature as consisting of massive maroon siltstone (e.g., Smith and Ward, 2001), the lithologies in the *Lystrosaurus* AZ now are reported as being either greenish-gray or maroon (Smith and Botha-Brink, 2014), diminishing the scale and extent of color alteration as originally reported and illustrated. The interpreted changeover in fluvial architectural style of the Karoo Basin is envisioned as a global phenomenon (Benton and Newell, 2014), as seasonally wet conditions transitioned to arid conditions, accompanied by the replacement of wide meandering channel regimes with low sinuosity river systems in the Palingkloof Member. With increasing aridity, these regimes were replaced by anabranching river systems developed in the post-extinction landscape. Anabranching regimes contain intraformational conglomerate, reworked from paleosols (Pace et al., 2009), as channel-lag deposits (Ward et al., 2000, 2005), and are considered distinctive of the Katberg Formation by some workers (Smith and Botha-Brink, 2014). Lenticular, thin intraformational conglomerate also is reported from the underlying uppermost Palingkloof Member, and has been interpreted as an indicator for the onset of rapid climate change prior to vertebrate turnover (Smith and Ward, 2001). The succession that transitions the *Daptocephalus* to *Lystrosaurus* AZs and, hence, includes the purported terrestrial PTB, has been placed into a magnetostratigraphic context by Ward et al. (2005) who compared their results with the estimated geomagnetic polarity time scale across the PTB, based largely on results from the marine succession.

The stratigraphic succession that transitions the vertebrate-defined PTB interval at Old (West) Lootsberg Pass is reported as consisting of 20 m of uppermost Permian and over 280 m of lowermost Triassic strata, based on magnetic polarity stratigraphy data, the documentation of which is extremely limited (Ward et al., 2000, 2005, their fig. 1). The physical location of Ward et al.'s (2000) reported section is important because they illustrate an ~25-m-thick greenish siltstone succession beneath their PTB, which is overlain by thick, maroon siltstone interbedded with thin sandstone. The reported GPS coordinates of their section are located between our measured sections [2] and [3] (Figs. 3, 11). Although Ward et al.'s (2000) GPS coordinates are not identified as representing either the section's base or top, their generalized stratigraphy conforms most closely to the succession of rocks in our transect [section 2] at a stratigraphic position beginning at ~52 m as marked in Figure 11. There is no other stratigraphic interval lower in the area near the published GPS coordinates of Ward et al. (2000) in which the characteristic rock types of this lithostratigraphic succession are exposed. Hence, as reported, Ward et al.'s (2000) section most likely lies in the *Lystrosaurus* AZ of the Katberg Formation and is not part of the Palingkloof Member (Figs. 10, 11). Ward et al. (2005) indicate the presence of a long normal polarity magnetozone of ~100 m thickness that is overlain by an 80-m-thick reverse-polarity magnetozone. These rocks are positioned stratigraphically above the PNC-bearing wacke in which previously we have placed the *Daptocephalus–Lystrosaurus* Assemblage Zone boundary (Gastaldo et al., 2015) using lithologic and paleontologic criteria of other workers (Ward et al., 2000, 2005; Smith and Botha-Brink, 2014; Botha-Brink et al., 2014; Viglietti et al., 2016). Data presented herein require a reevaluation of both the stratigraphic framework for this locality and the mag-

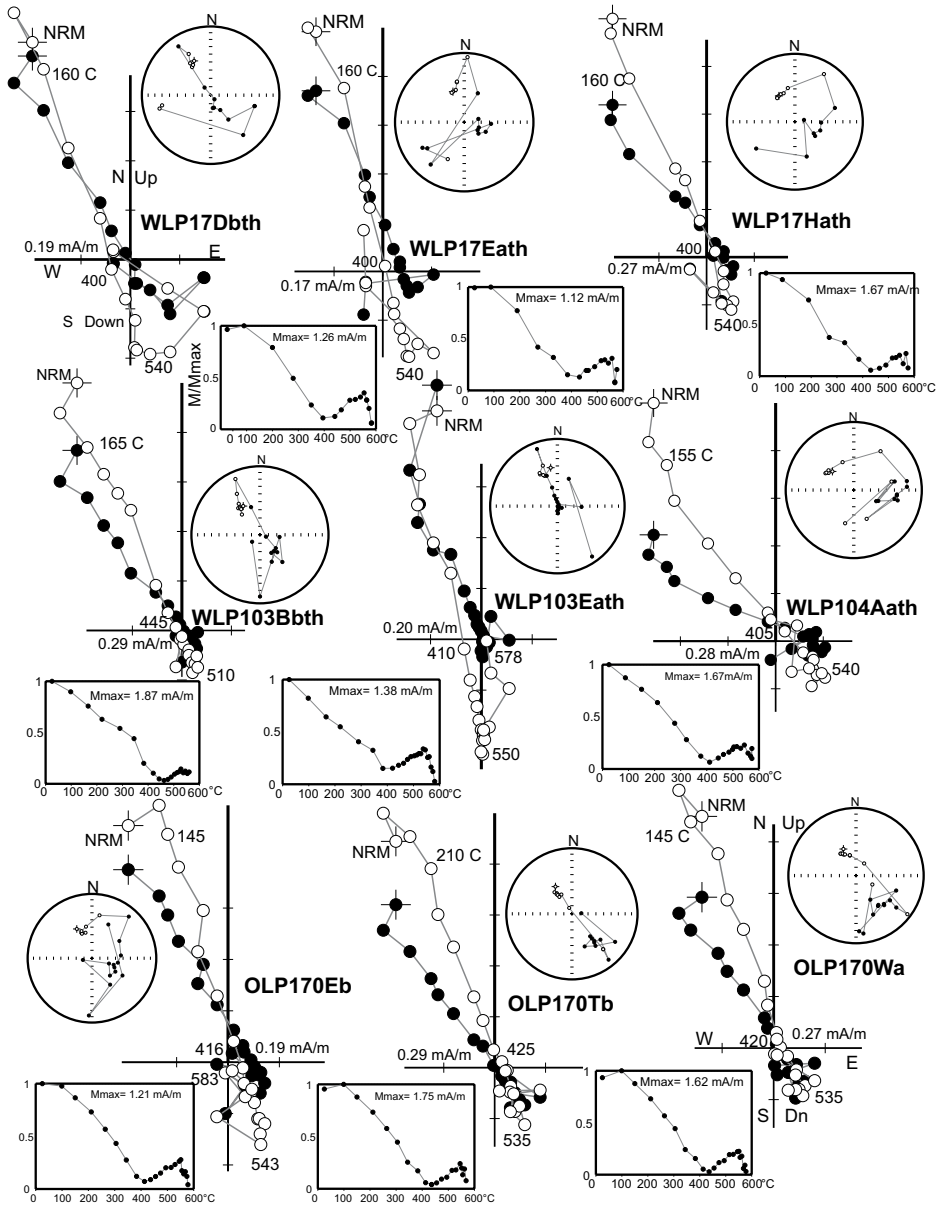


**Figure 13. Examples of orthogonal progressive demagnetization diagrams showing the end point of the magnetization vector plotted onto the horizontal (filled symbols) and vertical (open symbols) planes (NS-EW, EW-Up/Down) for individual specimens from samples from sites WLP17, WLP103, and WLP170. All samples taken at essentially the same stratigraphic interval and have been subjected to progressive thermal demagnetization. Demagnetization steps in temperatures (°C) are given alongside selected vertical projection data points. Also shown are normalized intensity decay plots showing response to progressive thermal or AF treatment (abscissa is peak temperature in °C, or alternating field, in milliTesla) and equal area stereographic projections of the magnetization vector measured at each step. Note that the coordinate (geographic) axes for each and every diagram are identical in orientation. NRM—natural remanent magnetization.**

netostratigraphic implications of this purported end-Permian boundary section when placed into a chronostratigraphic context.

### Implications of a Stratigraphic Framework at Old (West) Lootsberg Pass

Measured sections at Old Lootsberg Pass are dominated by fining up sequences on the order of a few meters to decameters in thickness (Figs. 10, 11). These are comprised of either yellow-gray wacke overlain by light olive-gray or olive-gray, coarse-and-fine siltstone, or fining up siltstone intervals, of which several are fossiliferous (Gastaldo et al., 2015, 2017). Reddish-gray mottling exists low in our composite section, but is restricted only to a <2 m interval beneath a concretion-bearing olive-gray siltstone (Fig. 10). Gastaldo et al. (2015) assign the underlying olive-gray rocks to the Elandsberg Member, and use the first appearance of this reddish-gray siltstone to identify the base of the lower Palingkloof Member following the recommendation of Johnson et al. (2006). We note that this criterion, which is currently used to distinguish between lithostratigraphic members may not be reliable due to the patchy spatial nature of reddish-gray siltstone in the area (Neveling et al., 2016a, 2016b; Gastaldo et al., 2017; Li et al., 2017). But, as currently accepted, the first occurrence of maroon mudrock lies beneath the transition from the *Daptocephalus* to the *Lystrosaurus* Assemblage Zone (Smith and Botha-Brink, 2014), and conforms to the widely accepted end-Permian model. However, what does not conform to the model is the presence of intraformational PNC deposits ~55 m below in the subjacent Elandsberg Member (Figs. 3, 10).

The presence of calcite-cemented, intraformational PNC conglomerate in the stratigraphically lowest channel-form wacke near the base of our section (Figs. 3, 10) demonstrates that degradational landscape processes (Gastaldo and Demko, 2011) operated long before the purported turnover in vertebrate assemblages. The PNC conglomerate (Fig. 5) appears at the base of the channel-fill succession, from which we report an Early Changhsingian U-Pb ID-TIMS age estimate (Gastaldo et al., 2015) that is ~1.6 Ma older than the globally accepted age of the PTB. Pace et al. (2009) present a climate-based model to explain the physical processes responsible for genesis of such intraformational PNC deposits.

Pedogenic calcite-cemented nodules originally formed in soil horizons of seasonally dry calcic-Vertisols or Calcisols that developed across a regional Karoo landscape. When either climate shifted back to more seasonally wet conditions or the area experienced a change in fluvial gradient (Gastaldo and Demko, 2011), or both, fluvial incision and lateral channel migration eroded and scavenged the calcic soils. Silt and clay were reworked and transported basinward resulting in renewed floodplain aggradation in another part of the Karoo Basin where Protosols formed (Gastaldo et al., 2014). Larger clasts, including pedogenic nodules, were concentrated in channel-lag deposits and, hence,

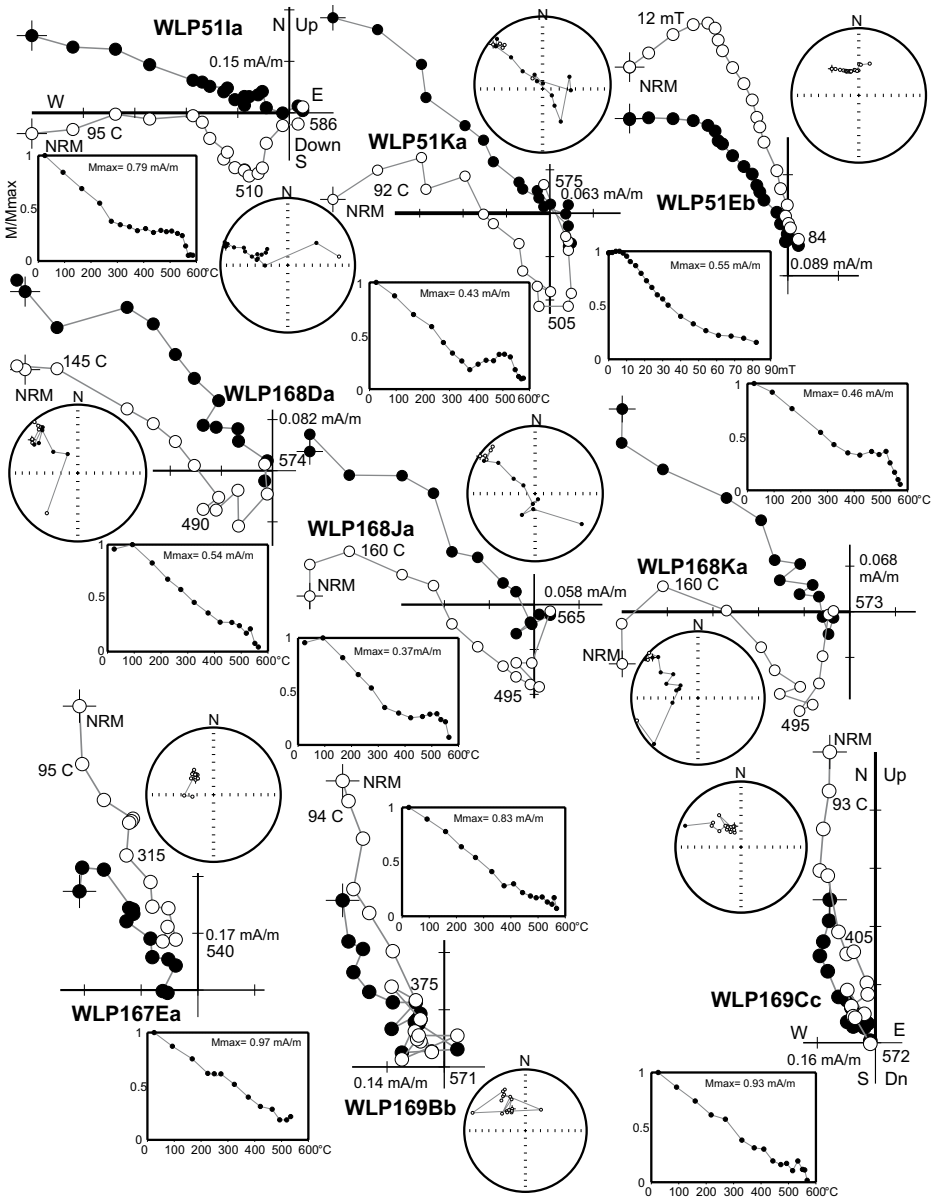


**Figure 14. Examples of orthogonal progressive demagnetization diagrams showing the end point of the magnetization vector plotted onto the horizontal (filled symbols) and vertical (open symbols) planes (NS-EW, EW-Up/Down) for individual specimens from samples from sites WLP51 and WLP168, both at the same stratigraphic interval, that have been subjected to progressive thermal or alternating field (AF) demagnetization. Also shown are selected examples from specimens from samples collected from sites immediately above and below the WLP51/WLP168 interval. Demagnetization steps in temperatures (°C) are given alongside selected vertical projection data points. Normalized intensity decay plots show response to progressive thermal or AF treatment (abscissa is peak temperature in °C, or alternating field, in milliTesla) and equal area stereographic projections of the magnetization vector measured at each step. Note that the coordinate (geographic) axes for each and every diagram are identical in orientation. NRM—natural remanent magnetization.**

serve as the only remnants of these seasonally dry soils in the record (Pace et al., 2009; Gastaldo and Demko, 2011). The mere fact that PNC-bearing, intraformational deposits occur in the Elandsberg Member demonstrates that processes, thought to be restricted to the interval of vertebrate turnover, occurred in the early Changhsingian, long before the purported biodiversity crisis. The occurrence of the PNC lithofacies low in the section at Old (West) Lootsberg Pass also negates the contention that this sedimentary feature is diagnostic of the Katberg Formation or the *Lystrosaurus* AZ (Ward et al., 2005; Smith and Botha, 2005; Botha and Smith, 2006; Smith and Botha-Brink, 2014).

Another aspect of the currently accepted vertebrate-turnover model that is not replicated by our observations and data from Old (West) Lootsberg Pass centers on the nature of the lithologies near, and coloration relative to, the vertebrate-biozone boundary interval. The extinction event in the Karoo Basin is reported to be marked by the presence of a 3–5-m-thick interval of maroon siltstone/claystone couplets with distinct, thick successions of reddish siltstone upsection (Smith and Ward, 2001; Ward et al., 2005; Smith and Botha-Brink, 2014). We find no such interval at the stratigraphic position at which Smith and Botha-Brink's (2014) vertebrate data indicate both the vertebrate-biozone turnover and the purported terrestrial PTB (Fig. 10; Gastaldo et al., 2017). Rather, their biozone boundary falls in a fining up succession characterized by olive-gray siltstone, above which is exposed only olive-gray siltstone for at least 10 m. Interbedded olive-gray and reddish-gray siltstone, the original description reported for the "unique" boundary event bed (Smith and Ward, 2001), is restricted to small spatially isolated exposures (Fig. 11; Li et al., 2017). This feature was acknowledged by Ward et al. (2012) but discounted, thereafter, with the contention that a single correlative and mappable bed can be used to identify the boundary (Smith and Botha-Brink, 2014; Botha-Brink et al., 2014; Viglietti et al., 2016). The interbedded lithofacies used by Ward et al. (2005) to mark the contact between their Unit I and II is exposed for less than a few meters laterally adjacent to the railroad (Fig. 11, section 2), some ~70 m higher than where it is reportedly placed by Smith and Botha-Brink (2014). In addition, we find that siltstone color varies spatially in correlative intervals, and that singly colored siltstone intervals cannot be traced laterally for more than, possibly, a few hundred meters (Fig. 11; Gastaldo et al., 2017; Li et al., 2017). This lateral variation in color is interpreted by Li et al. (2017) to be early diagenetic, with the authigenic genesis of very fine (micron-sized) hematite in these sediments. This is in contrast to an eolian origin for reddish silt as proposed by Smith and Botha-Brink (2014), for which Li et al. (2017) found no evidence in support of the interpretation. Several siltstone intervals are fossiliferous (Gastaldo et al., 2015, 2017), and include *Katbergia*-burrowed beds,

TABLE 1. U-Pb ISOTOPIC DATA FOR SINGLE CHEMICALLY ABRADED ZIRCON GRAINS FROM A SILICIFIED SILTSTONE, TROUGH FILL IN SECTION 12 (FIGS. 3, 10), OLD LOOTSBERG PASS, KAROO BASIN, SOUTH AFRICA

| No. | $Pb_C$ (pg) (a) | $Pb^*/Pb_c$ (b) | Th/U (c) | $^{206}Pb/^{204}Pb$ measured (d) | $^{207}Pb/^{235}U$ (e) | 2σ | $^{206}Pb/^{238}U$ (e) | 2σ | corr coef (f) | $^{207}Pb/^{206}Pb$ (g) | 2σ | Ages (Ma) $^{207}Pb/^{235}U$ (h) | 2σ | $^{206}Pb/^{238}U$ (g-h) | 2σ |
|---|---|---|---|---|---|---|---|---|---|---|---|---|---|---|---|
| z1 | 0.8 | 11.4 | 0.63 | 694 | 0.3293 | 0.0059 | 0.043491 | 0.000162 | 0.499 | 0.05491 | 0.00091 | 289.0 | 4.5 | 274.44 | 1.00 |
| z2 | 0.8 | 3.3 | na | 263 | 0.3023 | 0.0162 | 0.041324 | 0.000167 | 0.846 | 0.05305 | 0.00267 | 268.2 | 12.7 | 261.03 | 1.03 |
| z3 | 0.4 | 15.0 | 1.17 | 807 | 0.2922 | 0.0048 | 0.041187 | 0.000076 | 0.637 | 0.05145 | 0.00080 | 260.3 | 3.8 | 260.19 | 0.47 |
| z4 | 0.5 | 13.2 | 1.04 | 732 | 0.2914 | 0.0053 | 0.040700 | 0.000113 | 0.532 | 0.05192 | 0.00088 | 259.6 | 4.2 | 257.17 | 0.70 |
| z5 | 0.4 | 16.7 | 0.54 | 1033 | 0.2871 | 0.0044 | 0.040636 | 0.000099 | 0.499 | 0.05124 | 0.00073 | 256.3 | 3.5 | 256.78 | 0.61 |

*Note:* Zircon grains (z) pretreated by thermal annealing and Hf etching (chemical abrasion; Mattinson, 2005). na—not available.
(a) $Pb_C$ is total common Pb in analysis in picograms.
(b) $Pb^*/Pbc$ is ratio of radiogenic to common Pb.
(c) Th/U calculated from radiogenic $^{208}Pb/^{206}Pb$ ratio and $^{207}Pb/^{206}Pb$ age assuming concordance.
(d) $^{206}Pb/^{204}Pb$ measured ratio corrected for common Pb in spike and fractionation only.
(e) Pb/U ratios corrected for fractionation, common Pb in spike and blank. All common Pb assumed to be blank (blank isotopic composition: $^{206}Pb/^{204}Pb$: 18.22, $^{207}Pb/^{204}Pb$: 15.61, $^{208}Pb/^{204}Pb$: 39.36 [2σ errors of 1%]).
(f) Corr. coef. = correlation coefficient.
(g) Corrected for initial Th/U disequilibrium using radiogenic $^{208}Pb$ and Th/U[magma] = 4.2.
(h) Ages calculated using the decay constants $\lambda_{238}$ = 1.55125E-10 and $\lambda_{235}$ = 9.8485E-10 (Jaffey et al. 1971).

some of which represent paleosols (Gastaldo and Rolerson, 2008). But, coloration of these siltstone intervals is neither uniform nor spatially consistent over distances traced for <1 km.

## Geochronologic Implications

Ward et al. (2005) remarked that it was not possible, at that time, to place any geochronometric constraints on the transition between the *Dicynodon* and *Lystrosaurus* AZs due to the absence of datable deposits. This sentiment was echoed by Erwin (2006) after spending time in the Lootsberg Pass area, leaving chemostratigraphic and magnetostratigraphic data as the only potential means of a correlation with the marine record at Meishan, China. To date, we have collected eight zircon-bearing silicified siltstone or devitrified claystone samples from the area (Fig. 1), with samples having originated from both the *Daptocephalus* and *Lystrosaurus* AZs (unpublished data). Two high-resolution maximum depositional age dates are from the correlative stratigraphic sections we document at Old Lootsberg Pass, one of which previously was published by Gastaldo et al. (2015).

The maximum age of the zircon-bearing silicified siltstone (porcellanite) that is part of a channel-fill complex in the lowest PNC-bearing sandstone body (Figs. 3, 8, 10) is early Changhsingian (253.48 ± 0.15 Ma, 2σ). Stratigraphically higher, and recovered from a silicified siltstone in a trough-fill of a cross-bedded barform, is a population of detrital zircons with a maximum depositional age of early Wuchiapingian (256.80 ± 0.6 Ma, 2σ). We also have obtained an early Wuchiapingian maximum-age assignment for a population of detrital zircon from a devitrified claystone in the Tweefontein area (see footnote 1; unpublished data), which is positioned at an equivalent stratigraphic bed only 1.25 km to the southeast (S31°48.704′, E024°49.047′). In both instances, these deposits exhibit primary sedimentary structures that indicate bedload transport and emplacement (Fig. 9). In contrast, the well-silicified siltstone (porcellanite; Gastaldo et al., 2015) is massive and exhibits features characteristic of ashfall emplacement (Fig. 8D).

There is an inverse stratigraphic-age relationship between these two zircon-bearing units in the Old Lootsberg Pass area. The presence of a Wuchiapingian suite of zircons in a position above a bed with a younger Changhsingian age assignment intimates that the former is a reworked volcanogenic deposit with a provenance area likely in the Cape Fold Belt. Sediments in the closed, fully terrestrial Karoo Basin originated from their erosion and transport from within drainage networks to their final emplacement in depocenters. These rocks comprise the fluvial Beaufort and overlying Stormberg groups. We interpret the correlative beds, from which older age estimates originate, to represent reworking of older deposits into younger strata in response to landscape degradation in an area outside of their final depositional setting. And, the fact that at least two, stratigraphically correlative beds with the same maximum-age assignment exist within 1.25 km of each other provides a means to identify a depositional time horizon (equivalence) across the area.

## Magnetic Polarity Stratigraphy Implications

Justification for the placement of the Karoo PTB also has been based on magnetic polarity stratigraphy information and has been used to suggest a tentative correlation between the Old (West) Lootsberg Pass and Commandodrift Dam localities (Ward et al., 2005). The PTB is inferred to be positioned near the base of a normal polarity magnetozone (their N1) and assumes that the published polarity stratigraphy is based on a primary magnetization. Unfortunately, no paleomagnetic data are presented for the West Lootsberg Pass locality that can be convincingly used to define the base of the N1 magnetozone and, even more importantly, the existence of the underlying reverse polarity magnetozone (R1). The position of the R1 magnetozone is inferred based on a correlation with polarity data from the Commandodrift dam section (Ward et al., 2005) using an "event-bed" datum, notably, that cannot be traced in the basin (Gastaldo et al., 2009; Gastaldo and Neveling, 2012; Neveling et al., 2016a). Furthermore, the original report from the Commandodrift dam section also does not include any robust documentation of the presence of reverse polarity magnetizations in any of the samples collected.

In terms of a magnetic polarity stratigraphy for the Old (West) Lootsberg Pass composite section studied, to date, all sites (as thin stratigraphic intervals) that we have examined in sufficient detail, with the exception of two, show the presence of a normal polarity magnetization as the principal and only well-defined component of the NRM (Fig. 12). Both sites that do not conform to this pattern include a short stratigraphic interval underlying an erosional contact with a fluvial complex. These two intervals are sites WLP17 (and correlative to adjacent sites WLP103/WLP104/WLP170; Fig. 13) and WLP51 (and correlative to adjacent sites WLP168; Fig. 14). All samples from site WLP17 (and WLP103.104/170; Fig. 13) show the unblocking of a first removed normal polarity magnetization and then the consistent isolation of a remanence of south-southeast declination and moderate positive inclination (thus of reverse polarity) at temperatures above ~450 °C. Specimens from many, but not all samples from site WLP51 and WLP168 (Fig. 14) show a similar pattern. As noted above, few additional sites reveal a consistent hint of the presence of a magnetization that is south-directed and of moderate positive inclination (reverse polarity). But this

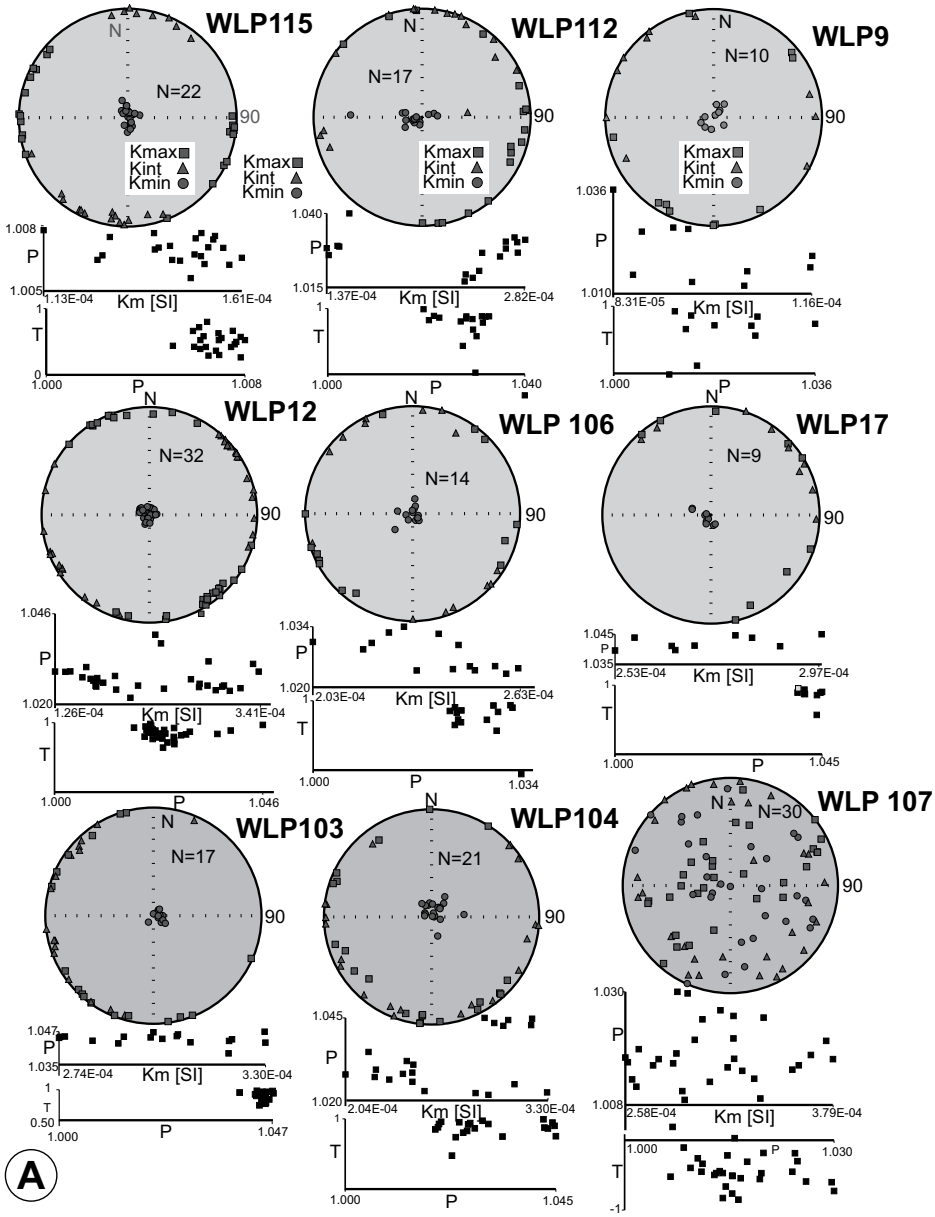


**Figure 15 (*on this and following page*). Examples of anisotropy of magnetic susceptibility (AMS) data from selected sites in the West Lootsberg Pass section, arranged in stratigraphic order from lowermost site selected (WLP115; A) to uppermost (WLP61; B). For each site, the stereographic projection shows the principal susceptibility axes for each specimen measured (lower hemisphere projections). In addition, the anisotropy parameter P, where P = Kmax/Kmin, is plotted versus bulk susceptibility for each specimen measured and the anisotropy parameter T, where T, the shape parameter ( = ([2lnKint – ln Kmax – lnKmin]/[lnKmax – lnKmin]) is plotted versus P. T values close to 1.0 are associated with strong oblate fabrics. The data from each site, with the exception of site WLP107, show a fabric that is typical of very fine grained detrital sedimentary rocks, with the minimum susceptibility axis essential vertical and well-grouped. Some sites (e.g., WLP21, WLP24, WLP29, and WLP61, all in coarser, fine sandstones versus typical siltstones) display a well-defined imbrication fabric, with the minimum susceptibility axis canted from the vertical. Site WLP107 was established in several 0.5 m + diameter concretions confined to a specific stratigraphic datum.**

magnetization, if it is of geologic significance, is typically a small percentage of the NRM and is often not well defined. The critical question, then, in the assessment of any paleomagnetic data from the Karoo Permian–Triassic sedimentary sequences is whether the normal polarity magnetization that is the principal component of the NRM in these rocks simply is a complete, or nearly complete, overprint or "remagnetization" associated with Karoo magmatism? Based on our ongoing magnetic polarity stratigraphy work on other upper Permian/lower Triassic sections in the Eastern Cape Province (e.g., Bethulie section, Free State Province), the most logical answer is that it is not. In some cases, the normal polarity magnetization is clearly completely unblocked at laboratory unblocking temperatures of ~450° C, if not well below, and a magnetization that is south-directed and of moderate positive inclination (interpreted as reverse polarity) is very well isolated at higher temperatures (Neveling et al., 2016a). Consistent with the observations of Lanci et al. (2013), normal polarity magnetizations that are isolated at laboratory unblocking temperatures above ~450° C are interpreted as early acquired, likely primary magnetizations. This interpretation is also consistent with the magnetic geothermometry work conducted by Maré et al. (2014), who, based on experiments on continuous drill core obtained at several localities in the Karoo Basin, concluded that sedimentary strata of the Karoo Supergoup experienced maximum temperatures between ~200° C and ~650° C, presumably prior to and during the time of Karoo Large Igneous Province magmatism. The highest maximum temperatures were derived from rocks within the (narrow) thermal aureoles of Karoo sills. For sedimentary strata spatially removed from and between sills, Maré et al. (2014) reported lower estimated maximum temperatures between 200° and 300° C. They also emphasized that their work implies that Karoo sill intrusion "did not completely overprint the magnetic signatures of Karoo sedimentary strata (Maré et al., 2014, p. 11)." In an independent approach, Flowers and Schoene (2010) reported apatite and titanite (U-Th)/He thermochronometric data from Precambrian crystalline rocks of the eastern Kaapvaal craton, nonconformably overlain by Lower Permian Ecca Group strata. The simulated time-temperature (t-T) paths derived from these data led these workers to conclude that peak Mesozoic temperatures (at the time of Karoo magmatism) were limited to less than or equal to ~175 °C. Thus, we conclude, given the available data and our present sampling coverage, that the sedimentary strata of the Old (West) Lootsberg Pass section we re-

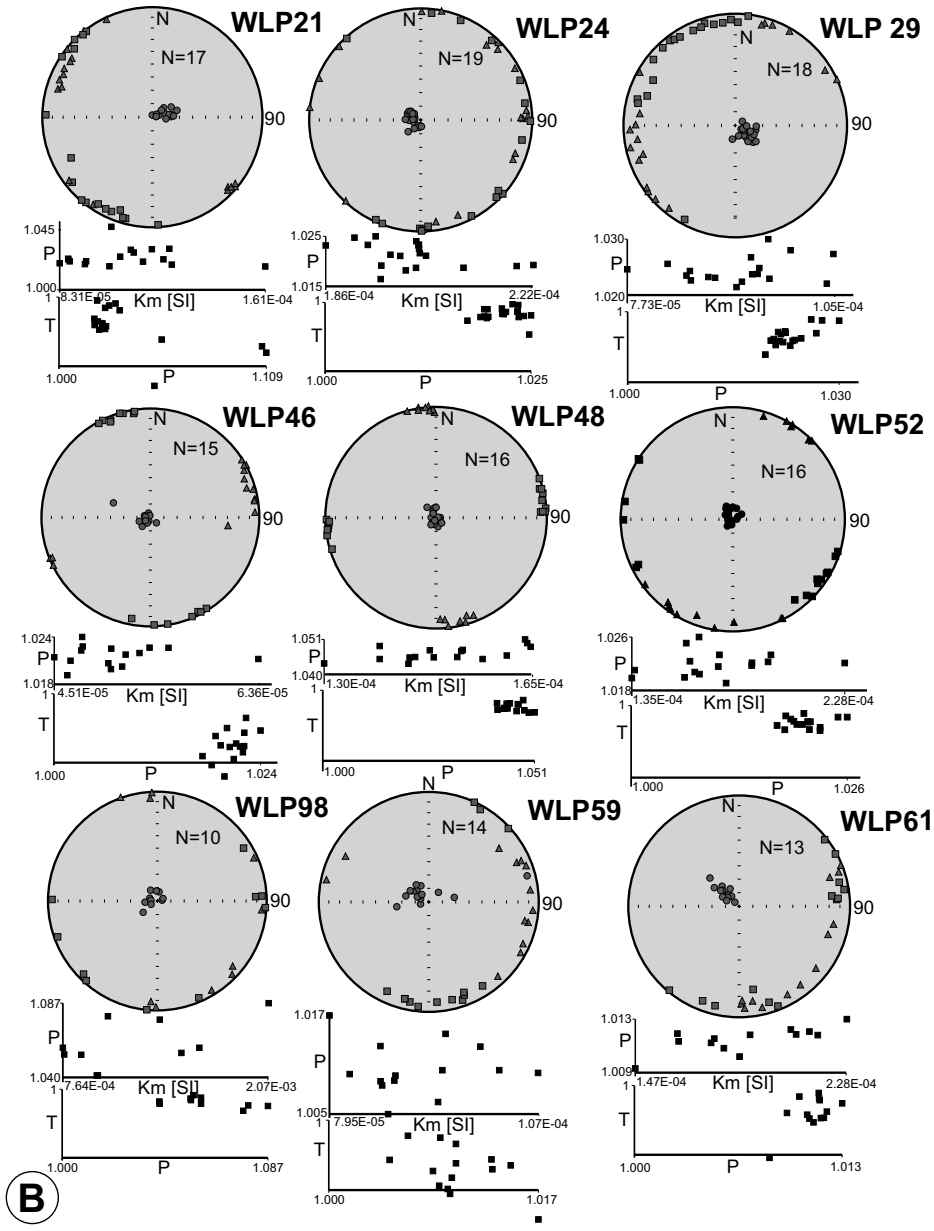


**Figure 15 (*continued*).**

port on in this paper do contain early acquired magnetizations and that these strata lie largely within several magnetozones of normal polarity or, thus, were deposited over a time interval dominated by normal polarity chrons. Intervening intervals during which time sediments accumulated during reverse polarity, on the other hand, are cryptic and were likely relatively short in duration.

The two stratigraphic intervals in which a primary signal of reverse polarity exists are less than 4.5 m in exposed total thickness, and each is in an erosional contact with an overlying thick fluvial sandstone. The 3.6-m-thick interval directly underlying the PNC-bearing sandstone as a datum by Gastaldo et al. (2015) is particularly cryptic (Fig. 18). Here, a thin, planar grayish-white sandstone is overlain by dark-gray and olive-gray siltstone (sites WLP51 and WLP168) across an exposure of ~6 m of lateral distance in a donga. These rocks are not exposed elsewhere in the area because the unit is covered by vegetation. The siltstone interval in which the reverse polarity signal is preserved is incised by another thin-bedded, fine to very fine, quartz sandstone body which serves as the base of the datum used by Gastaldo et al. (2015). The siltstone is medium-bedded and lenticular in geometry, and is laterally equivalent to a pedogenically altered siltstone to the north, which is interpreted as interfluvial deposits of an older landscape. Hence, the recognition of reverse polarity intervals at Old (West) Lootsberg Pass, and/or in other terrestrial dominated successions, easily could be missed when collection intervals are widely spaced, when the density of sampling at any interval is too low, and/or stratigraphic relationships are homogenized in a sampling strategy. Our recognition of short intervals of reverse polarity remanence is in stark contrast to previously reported magnetic polarity stratigraphy information for these rocks.

Ward et al. (2005) report a long reverse polarity magnetozone for their section at Old (West) Lootsberg Pass which, as noted above, lies in the Katberg Formation and begins a short stratigraphic distance below the railroad cut (Figs. 3, 10, 11). Here, their figure (Ward et al., 2005, their fig. 1) shows polarity data for 45 samples that originate from over 200 m of stratigraphic section dominated by maroon siltstone. The lowermost 100 m of the section published by Ward et al. (2005) conforms to the same interval in our measured section beginning at a stratigraphic height of ~142 m (Fig. 10). Although we have not encountered physical evidence for sampling from one of the more than 20 beds from which their oriented samples were collected in this interval, our data are in agreement with theirs in that this stratigraphic interval is dominated by normal polarity magnetozones. To date, we have no data available with which to confirm the presence of a long interval of reverse polarity higher in the section.

## Old (West) Lootsberg Pass and the Continental end-Permian model

Our multifaceted observations and data from Old (West) Lootsberg Pass contradict many of the attributes of this section reported to transition the terrestrial Permian–Triassic boundary in the Karoo Basin. These include: the basic stratigraphic succession, lithofacies associations, and lateral lithofacies relationships; the magnetostratigraphy ascribed to these rocks; and their chronostratigraphic placement in the very latest Permian.

The lithology reported to characterize the transition between the *Daptocephalus* and *Lystrosaurus* AZs, an interlaminated greenish-gray and maroon siltstone (Facies C of Smith and Botha-Brink, 2014), is not associated with the stratigraphic position at which the vertebrate turnover is identified (Gastaldo et al., 2017). This interlaminated interval, reported to be mappable across the basin and used by various workers to locate the vertebrate-defined end-Permian extinction event (Botha-Brink et al., 2014; Rubidge et al., 2016; Viglietti et al., 2016 and others),

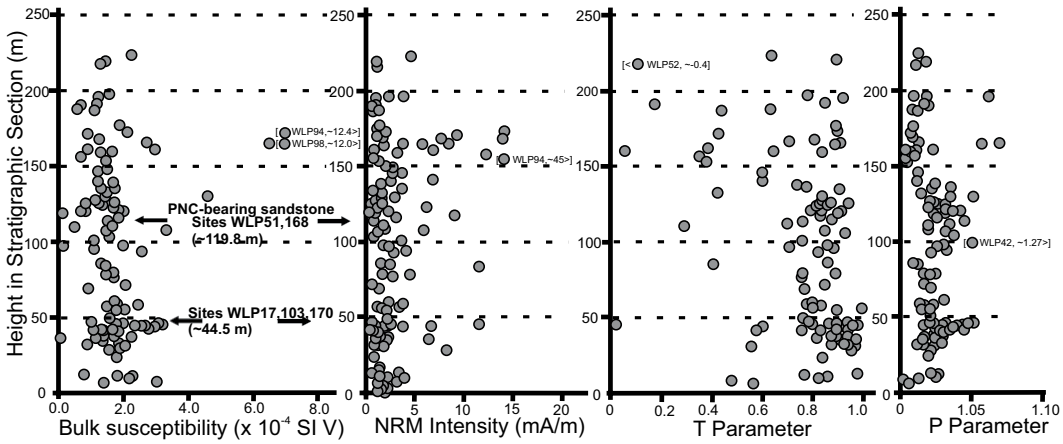


**Figure 16. Compilation of magnetic susceptibility, remanence intensity, and anisotropy of magnetic susceptibility parameter data for most of the sampling sites established for this study. Each data point represents the mean value of data from specimens from multiple independent samples (typically at least seven) measured at each site. NRM is the natural remanent magnetization. The T parameter is Jelinek's (1981) shape parameter for the susceptibility magnitude ellipsoid, where a T value of +1 is for a perfectly oblate ellipsoid, a T value of 0 is neutral, and a T value of –1 is for a perfectly prolate ellipsoid. P is the anisotropy degree (Kmax/Kmin). PNC—pedogenic nodular conglomerate.**

is not isolated to a single correlative horizon (Fig. 11), a fact previously acknowledged by Ward et al. (2012). Rather, this lithofacies is found spatially isolated at several discrete horizons higher in our stratigraphic framework (Li et al., 2017), two localities of which are in the Katberg Formation (Fig. 11). The interlaminated interval identified as the PTB by Ward et al. (2000, 2005), and used by them as the lithostratigraphic datum at Old Lootsberg Pass is positioned, in fact, adjacent to the railroad cut ~70 m stratigraphically above where Smith and Botha-Brink (2014) place their PTB based on their vertebrate biostratigraphy (Gastaldo et al., 2017). Additionally, the same facies is found at several different stratigraphic positions in the area (Fig. 11). The physical relationships of Facies C of Smith and Botha-Brink (2014) are no different at Old Lootsberg Pass than what Gastaldo et al. (2009) demonstrated at Bethulie and subsequently acknowledged by Ward et al. (2012). The interlaminated greenish-gray and reddish-gray (maroon) siltstone lithofacies is spatially and temporally isolated in successive landscapes, and cannot be used as a lithologic criterion to identify the boundary between vertebrate biozones. Our current observations only reinforce Ward et al.'s (2012) conclusion that the lithology is neither unique nor mappable, and cannot be used as a datum on which to identify the PTB. And, our current sedimentologic data demonstrate that a non-unique feature of purported post-extinction river systems. Rather, the interlaminated lithofacies represents channel-fill successions in a fluvial setting (Li et al., 2017).

Smith and Botha-Brink (2014) use the presence of intraformational (PNC) conglomerate, composed of mud-pebble clasts, reworked bone, and spheroidal pedogenic pisoliths found as channel-lag deposits, as a distinctive feature of their Facies E and the Katberg Formation. Sandstone bodies with these characteristics are reported to be restricted to the *Lystrosaurus* AZ, formed under an arid climate, and indicative of post-extinction times. We have documented the presence of PNC lag deposits in the Elandsberg Member (*Daptocephalus* AZ; Fig. 10) in the basal sandstone body from which an early Changhsingian maximum age has been acquired (Gastaldo et al., 2015). The occurrence of PNC-bearing channel-lag deposits indicates that the process proposed by Pace et al. (2009) to explain these intraformational conglomerates began operating earlier in time, and is not a unique feature of the *Lystrosaurus* AZ. As such, the presence of this intraformational conglomerate lithofacies is not a consequence of increasing aridification coincident with a change in vertebrate fauna as interpreted by many workers (Smith and Ward, 2001; Smith and Botha-Brink, 2014). The presence of PNC deposits throughout the section indicates an increased

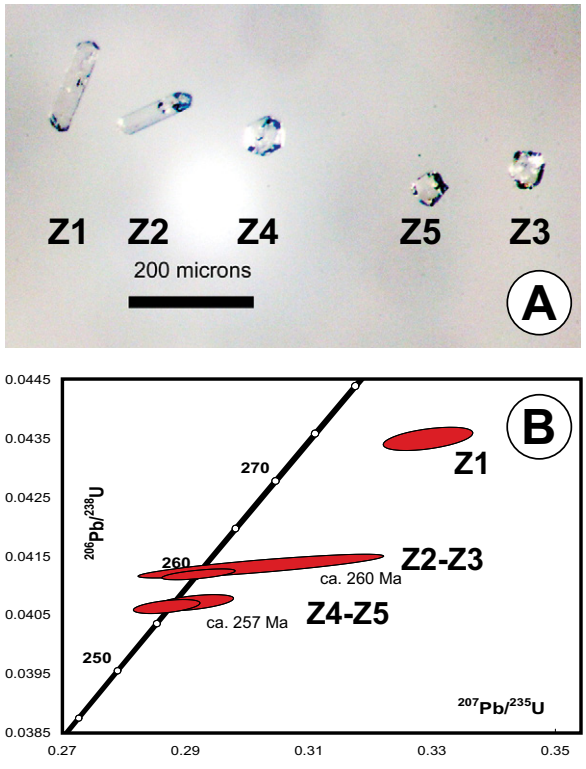


**Figure 17. Concordia diagram showing U-Pb data for five chemically abraded single zircon grains from a silicified siltstone trough-fill ~40 m below the purported Permian–Triassic boundary, as identified by Smith and Botha-Brink (2014) in our Old Lootsberg Pass section, Karoo Basin, South Africa, with the youngest grain dated at 256.3 ± 0.6 Ma (2σ). Inset is a photomicrograph of representative zircon grains similar to those that were analyzed.**

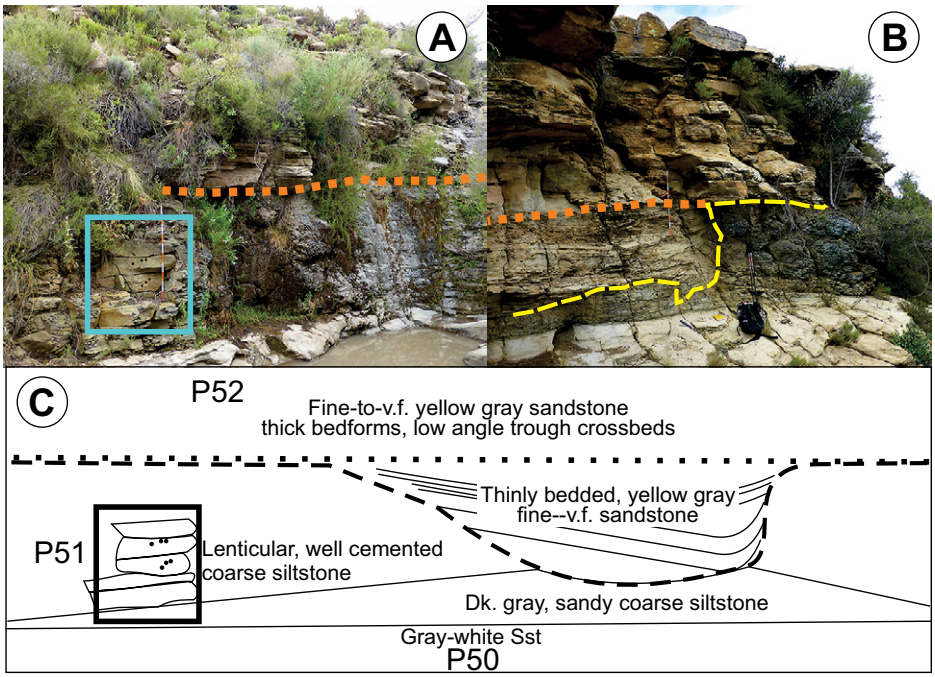


**Figure 18. Physical relationship of paleomagnetic sampling sites WLP50–WLP52 over ~3 m of stratigraphy at the base of the datum sandstone used by Gastaldo et al. (2015, 2017; see Figs. 10, 11 [section 5]). (A) Outcrop on northwest wall of donga exposure showing upper contact of the gray-white sandstone (P50) overlain by an interval of lenticular, well-cemented coarse siltstone beds (blue box; paleomagnetic sampling sites WLP51 and WLP168). Erosional contact with overlying pedogenic nodular conglomerate–bearing wacke used by Gastaldo et al. (2015) as a datum is shown as an orange dotted line. Scale in decimeters. (B) Outcrop ~8 m on northeast side of donga exposure showing upper contact of the gray-white sandstone (P50) overlain by a dark-gray, sandy, coarse siltstone into which a thin laminated, low-angle crossbedded sandstone is incised (yellow dashed line) and is overlain by the same erosional contact found in A (orange dotted line). (C) Line illustration of the outcrop and physical relationships between sample sites P50 (normal polarity), P51 (reverse polarity), and P52 (normal polarity). Not to scale; v.f.—very fine.**

frequency of climate flux over time and landscape response (Neveling et al., 2016a), and that local-and-regional landscape response cannot be ascribed to a change in siltstone color.

The current model for rocks transitioning the *Daptocephalus* to *Lystrosaurus* AZs and, hence, the vertebrate-defined terrestrial PTB as currently defined (Viglietti et al., 2016; Rubidge et al., 2016), is one in which a reddening of siltstone color is interpreted to be in response to increasing aridity. Lateral lithofacies relationships at Old Lootsberg Pass (Fig. 11) demonstrate that contemporaneous deposits vary in coloration from variants of olive-gray, to mottled of end member colors, to reddish-gray over short geographic distances (Li et al., 2017). Olive-gray siltstones in which impressions of *Glossopteris* leaves are preserved (Gastaldo et al., 2015, 2017) are lateral correlatives to reddish-gray siltstone in which vertebrate remains occur. And, where siltstone reddening is found, color modification is the result of authigenic, micron-sized hematite and maghemite coatings on clay minerals (Li et al., 2017) rather than through the introduction of loessic hematite crystals as proposed (Smith and Botha-Brink, 2014). Using a multifaceted data set, Li et al. (2017) conclude that authigenic hematite was early diagenetic in origin and formed in response to oxidation state flux in sediment-pore waters, and was not related to a change in climate. Their conclusion follows many other authors: that color alteration is not a function of climate nor an indicator of aridification (e.g., Sheldon, 2005; Kraus and Hasiotis, 2006).

The magnetostratigraphic record of our study interval demonstrates the presence of at least two reverse polarity magnetozones and, thus, that a plausible interpretation is that the composite section at Old Lootsberg Pass includes three (longer) normal polarity chrons with two (short) reverse polarity chrons. Each reverse polarity magnetozone is stratigraphically restricted to a short section of mudrock situated beneath an erosional contact with an overlying fluvial complex and, thus, is cryptic in character as we cannot determine how temporally significant are the reverse polarity magnetozones. In the case of the upper channel complex, the reverse polarity magnetozone (WLP51, WLP168) is in rocks found in a small exposure lateral to the base of the incised channel (Fig. 18). In this case, the fluvial channel is characterized at its base by the presence of PNC (due to restricted exposure of the sandstone above WLP17, it is not possible to document a similar case). This relationship strengthens Pace et al.'s (2009) proposed model for aggradational and degradational shifts in the fully terrestrial landscape in this part of the Karoo Supergroup, with most of the reverse polarity magnetozones lost due to erosion associated with a change in fluvial gradient or climate flux (Gastaldo and Demko, 2011). These relationships demonstrate that, contrary to published reports of a stratigraphically continuous record across the *Daptocephalus* to *Lystrosaurus* AZ's (Smith, 1995; Ward et al., 2000, 2005; Smith and Ward, 2001; and others), our magnetostratigraphic evidence can be interpreted to indicate the presence of gaps in the stratigraphy. The number of identified reverse magnetozones is critical to estimating how close the accepted vertebrate-assemblage zone boundary may be to the end-Permian crisis in the marine realm.

The paleomagnetic data we report here that permit the construction of a tentative magnetic polarity stratigraphy for the WLP/OLP stratigraphic section in no way contradict or are inconsistent with our general understanding of the geomagnetic polarity time scale across the Permian/Triassic boundary. Szurlies (2013) reports five reverse polarity chrons between ca. 253.8 Ma and the interpreted position of the PTB (Fig. 19). Hounslow and Balabanov (2016) reported at least three reverse chrons between ca. 253.8 and their interpreted position of the PTB directly at the base of a long normal polarity chron (Fig. 19). At present, we are not able to directly correlate either reverse polarity magnetozone that we have documented in this contribution with any established/published geomagnetic polarity time scale across the PTB. We emphasize that the OLP section is dominated by normal polarity magnetozones and that the potential placement of the PTB within the Katberg Formation is not inconsistent with the available magnetic polarity stratigraphy data that we have obtained and reported.

Szurlies (2013) compiled a Late Permian to Early Triassic magnetic polarity time scale that includes three short reversal polarity chrons fol-

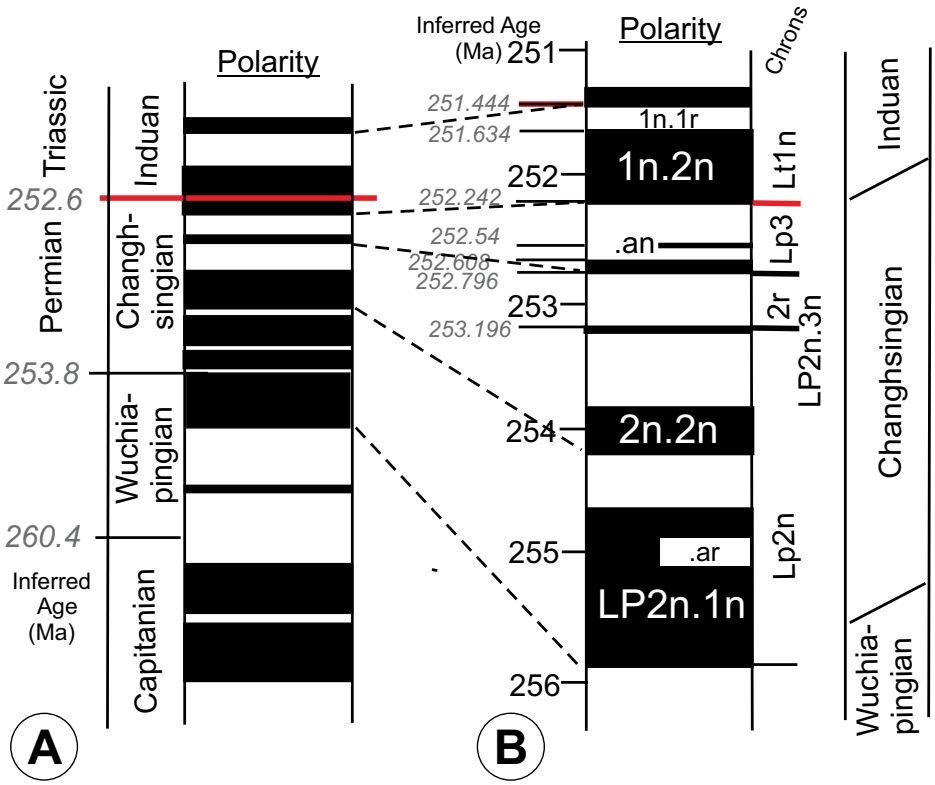


**Figure 19. Estimates of the geomagnetic polarity time scale from the Late Permian to earliest Triassic, modified from (A) Szurlies (2013) and (B) Hounslow and Balabanov (2016). Inferred ages for stage boundaries (A) or for the start and/or end of specific polarity chrons (B) are taken directly from the original publication and have not been modified as a result of more recent reports. Black (white) refers to normal (reverse) polarity chrons. Labeled polarity chrons in (B) are directly from the source. Note that the vertical (inferred age) scales are different for (A) and (B). Dashed lines represent our attempt to correlate the bases of key normal polarity chrons. Note that in (A), the Permian/Triassic boundary is placed within a normal polarity chron, estimated by Szurlies (2013) to be ~700 ka in duration. In (B), the Permian/Triassic boundary is placed at the base of a normal polarity chron, estimated to be ~600 ka in duration.**

lowed by longer normal polarity chrons in the early Changhsingian (Fig. 19A). Thereafter, a longer reverse chron is followed by a short normal chron which, in turn, is followed by a longer reverse chron. It is this long reverse chron that Ward et al. (2005) correlated with their R1 magnetozone using data from Old Lootsberg Pass. This reverse polarity chron is succeeded by what Szurlies (2013) estimated to be a ca. 700 ka duration normal polarity chron in which the end-Permian event is located in the marine record. The more recently reported polarity time scale for this time interval by Hounslow and Balabanov (2016; Fig. 19B) is similar in overall structure, but shows the predominance of reverse polarity chrons in the late Changhsingian and places the boundary between the Changhsingian and the Induan (PTB) at the base of a long (~600 ka duration) normal polarity chron, rather than within it. The presence of only two reverse polarity magnetozones at Old (West) Lootsberg Pass in a 60 m (based on vertebrate data of Smith and Botha-Brink, 2014) or ~75 m (Gastaldo et al., 2015, 2017) stratigraphic section, in conjunction with an early Changhsingian age maxima, derived from a well silicified porcellanite, strengthen Gastaldo et al.'s (2015) interpretation that this stratigraphic section and, by extension, the record encompassing the transition from the *Daptocephalus* to *Lystrosaurus* AZ's, is not coeval with events in the latest Permian in the marine realm. If the Old (West) Lootsberg Pass succession was time equivalent with marine sequences deposited prior to, during, and after the end-Permian extinction event, we would expect to have identified four intervals of reverse-to-normal polarity chrons, possibly dominated by reverse polarity if the compilation of Hounslow and Balabanov (2016) is more viable, in this short section of rock. We have not.

## CONCLUSIONS

The lithostratigraphic section exposed at Old (West) Lootsberg Pass in the Eastern Cape Province of South Africa serves as a cornerstone for the currently accepted model of biodiversity loss during the end-Permian crisis. Previous workers have combined litho- and biostratigraphy, along with magnetostratigraphic data, in support of an extinction model for terrestrial ecosystems interpreted to be coeval with the events in the marine realm (Ward et al., 2000, 2005; Smith and Ward, 2001; Smith and Botha-Brink, 2014; and others). Based on the assumption that a complete Permian–Triassic stratigraphic record transitions the *Daptocephalus* (formerly *Dicynodon*; Viglietti et al., 2016) to *Lystrosaurus* Assemblage Zones, criteria to delineate the Permian–Triassic boundary by these workers here, and at other localities, include: a unique facies assemblage associated with the PTB; a change in both siltstone color and fluvial architectural styles interpreted to represent an increasingly arid climate trend; the presence of a normal polarity chron, located above a reverse polarity chron associated with the unique boundary facies; and the occurrence of intraformational conglomerate in the post-extinction, *Lystrosaurus* AZ in response to a climate trend interpreted to be responsible for the demise of vegetation and consequent collapse, and rapid recovery, of the vertebrate fauna. Our multidisciplinary data set from this locality does not support many, if not all, of these interpretations.

We present a stratigraphic framework for Old (West) Lootsberg Pass that consists of twelve measured sections, physically correlated in the field using thick and extensive sandstone bodies as datums, encompassing more than 740 m of rock. These data are combined with a magnetostratigraphy, derived from a composite stratigraphic section of 240 m, in which two U-Pb ID-TIMS maximum-age estimates help to geochronometrically constrain the rocks. Combining these data, we conclude the following.

The rocks at Old Lootsberg Pass, which includes the Elandsberg and Palingkloof members of the Balfour Formation and overlying Katberg Formation, as currently defined, are not a record of continuous sedimentation as proposed (Smith, 1995; Smith and Botha, 2005; Smith and Botha-Brink, 2014, and others). We have found sedimentologic evidence for the presence of intraformational pedogenic-nodule conglomerate at the base of sandstone bodies in the Elandberg Member, ~80 m below the vertebrate-defined boundary of Smith and Botha-Brink (2014), which indicates that degradational processes in response to fluxes in climate (Pace et al., 2009; Gastaldo and Demko, 2011) oper-

ated much earlier in the Changhsingian. Hence, the presence of pedogenic-nodule conglomerate cannot be considered diagnostic of the post–boundary rocks of the Katberg Formation, as the lithofacies is not temporally unique. As we reported elsewhere (Gastaldo et al., 2009; Neveling et al., 2016a, 2016b; Li et al., 2017), we have found that intervals of interlaminated greenish-gray and reddish-gray siltstone occur at several stratigraphic positions and these rocks are not a unique lithofacies that can be used to identify a time-correlative and mappable unit (Smith and Ward, 2001; Ward et al., 2005; Smith and Botha-Brink, 2014; Botha-Brink et al., 2014) in the basin. We have found that the one interlaminated interval reported by Ward et al. (2005) as their boundary facies crops out in the Katberg Formation some 70 m above where Smith and Botha-Brink (2014) place their PTB using vertebrate biostratigraphy and have demonstrated them to represent channel-fill deposits (Neveling et al., 2016a; Li et al., 2017). Similarly, we have found that there is no temporal or spatial character with respect to changeover in siltstone color (Li et al., 2017). Lateral relationships between greenish-gray and reddish-gray siltstone intervals in the Katberg Formation demonstrate them to be time equivalent and coeval facies. The presence of the PNC facies in the Elandsberg Member indicates that early Changhsingian landscapes in the Karoo Basin experienced a series of aggradational and degradational processes, resulting in a non-continuous sedimentary record that encompasses the upper part of the *Daptocephalus* and overlying *Lystrosaurus* AZs. Aggradational phases dominate over degradational phases, an observation witnessed with the integration of magnetostratigraphic data.

We have assessed the magnetic properties of (128) competent beds over a stratigraphic interval of 220 m and find that a normal polarity chron signature dominates the succession. A signature of reverse polarity chrons is observed in only two, short stratigraphic intervals of siltstone, both of which underlie sharp, erosional contacts with thick fluvial sandstone bodies in which a normal polarity signature exists. The fact that reverse polarity chron signatures only are found in two-siltstone successions, each of which is <3 m thick, further supports the interpretation that the rocks at Old Lootsberg Pass do not reflect a continuous sedimentary record. These rocks represent sedimentary processes and deposition during the early Changhsingian, as the magnetic polarity pattern is more compatible with that recorded elsewhere during the same chronostratigraphic succession.

Gastaldo et al. (2015) report an early Changhsingian age for a silicified siltstone in a channel-fill succession low in the section (Figs. 8, 10). Here, we report a maximum-detrital Wuchiapingian depositional date (Fig. 17) from a horizon in a stratigraphically higher sandstone body at Old Lootsberg Pass and a correlative claystone at Tweefontein (see footnote 1; Fig. 1). The Changhsingian-age estimate from our porcellanite originates from a thin, planar silicified porcellanite without evidence of primary bedload structures, whereas the Wuchiapingian detrital data originates from a siltstone lenticular-trough fill in a channel barform (Fig. 9). This indicates that these detrital grains had been eroded and reworked somewhere closer to the Cape Fold Belt as a consequence of physical processes operating in the drainage network of the provenance area. The presence of a younger zircon population in planar, channel-fill deposits that exhibit features consistent with ashfall emplacement, subjacent to a detrital zircon population of Wuchiapingian age, helps to confirm our interpretation that the upper *Daptocephalus* AZ is early Changhsingian. The magnetostratigraphic record also strengthens our interpretation.

The global composite magnetostratigraphy of Szurlies (2013) for the uppermost Permian and lowermost Triassic consists of a succession of ten normal-to-reverse polarity chrons, with a lower boundary age of 254.14 ± 0.7 Ma for the Changhsingian stage. The Changhsingian age estimate of Gastaldo et al. (2015) of 253.48 ± 0.15 places the porcellanite in the earliest quarter of the stage. As such, we would expect to encounter at least four, if not six, normal-to-reverse polarity intervals in the rocks at Old Lootsberg Pass if the 60 m of stratigraphy were equivalent to the 1.6 million years required if the *Daptocephalus*/*Lystrosaurus* AZ boundary was contemporaneous with the marine event, as suggested by Viglietti et al. (2016) and others. We have no physical, magnetic or geochronometric evidence to support equating the vertebrate turnover in the Karoo Basin with the end-Permian crisis in the oceans. Hence, we conclude that the turnover from the *Daptocephalus* to *Lystrosaurus* AZs is not coincident with the end-Permian marine event based on multidisciplinary evidence at Old (West) Lootsberg Pass.

Continental successions are notoriously incomplete as a consequence of a shifting balance between aggradational and degradational processes operating across the landscape (Pace et al., 2009; Gastaldo and Demko, 2011). Many fully terrestrial stratigraphies have been claimed to represent near continuous sedimentation (aggradation) with the acknowledgment of diastems or disconformities (degradation) normally expected in fluvial sequences (e.g., Smith and Ward, 2001; McElwain et al., 2007). As demonstrated here, such an approach is an oversimplification. The only way in which shifts in sedimentation patterns, the response of biological systems (i.e., turnover, extinction, recovery), and the magnitude of missing time any can be assessed in such complex successions is when, preferably, there is both a geochronometric and a high-resolution, tightly constrained magnetostratigraphic context. When either one or both are missing, patterns interpreted to represent sudden changes in processes that operated either in the lithosphere or biosphere may, rather, be a function of condensed sections and/or missing time, as demonstrated by the presence of cryptic reverse magnetozones in the current study. Hence, extreme caution is urged when extrapolating interpreted patterns across continents, hemispheres, and globally that are not constrained by such context.

**ACKNOWLEDGMENTS**

The authors appreciate the hospitality and kindness shown to them over past decade by: Justin and Liesl Kingwill, Blaauwater Farm; and JP and Hester Steynberg, Ganora Guest Farm. Field assistance by E.H. Gastaldo, R. Prevec (The Albany Museum), A. Ndhukwani and S. Makubalo (Council for Geoscience), and S. Cusack, J. Li, K. Lipshultz, and T. Sasajima (Colby College) are acknowledged. Laboratory assistance by B. Lycka, K. Ables, and M. Anekwe (University of Texas at Dallas) is greatly appreciated. Research efforts were supported, in part, by: the Council for Geoscience (South Africa); National Science Foundation EAR 0749895, 0934077, 1123570 and 1624302; a Fulbright Scholar Award from the U.S. Department of State to RAG; and Faculty Start-Up Support from the University of Texas at Dallas to JWG. Permit to collect palaeontological material at Blaauwater issued by ECPHRA to R. Prevec; permit number: 2/2/APM-PERMIT/13/08/001. Shu-Zong Shen and Jörg W. Schneider are thanked for reviews that strengthened the final manuscript.

**REFERENCES CITED**

Baresel, B., Bucher, H., Brosse, M., Cordey, F., Guodun, K., and Schaltegger, U., 2017, Precise age for the Permian-Triassic boundary in South China from high precision U-Pb geochronology and Bayesian age-depth modelling: Solid Earth Discussion, v. 8, p. 361–378, https://doi.org/10.5194/se-8-361-2017.

Benton, M.J., and Newell, A.J., 2014, Impacts of global warming on Permo-Triassic terrestrial ecosystems: Gondwana Research, v. 25, p. 1308–1337, https://doi.org/10.1016/j.gr.2012.12.010.

Botha, J., and Smith, R.H.M., 2006, Rapid vertebrate recuperation in the Karoo Basin of South Africa following the End-Permian extinction: Journal of African Earth Sciences, v. 45, p. 502–514, https://doi.org/10.1016/j.jafrearsci.2006.04.006.

Botha, J., and Smith, R.H.M., 2007, *Lystrosaurus* species composition across the Permo–Triassic boundary in the Karoo Basin of South Africa: Lethaia, v. 40, p. 125–137, https://doi.org/10.1111/j.1502-3931.2007.00011.x.

Botha-Brink, J., Huttenlocker, A.K., and Modesto, S.P., 2014, Vertebrate Paleontology of Nooitgedacht 68: A *Lystrosaurus maccaigi*-rich Permo-Triassic Boundary Locality in South Africa, *in* Kammerer, C.F., Angielczyk, K.D., and Fröbisch, J., eds., Early Evolutionary History of the Synapsida, Vertebrate Paleobiology and Paleoanthropology: Dordrecht, Springer, p. 289–304, https://doi.org/10.1007/978-94-007-6841-3_17.

Broom, R., 1906, On the Permian and Triassic Faunas of South Africa [Decade V]: Geological Magazine, v. 3, p. 29–30, https://doi.org/10.1017/S001675680012271X.

Broom, R., 1911, On some New South African Permian Reptiles: Proceedings of the Zoological Society of London, v. 81, p. 1073–1082, https://doi.org/10.1111/j.1096-3642.1911.tb01976.x.

Burgess, S.D., Bowring, S., and Shen, S.Z., 2014, High-precision timeline for Earth's most severe extinction: Proceedings of the National Academy of Science of the United States of America, v. 111, p. 3316–3321, https://doi.org/10.1073/pnas.1317692111.

Clapham, M.E., and Payne, J.L., 2011, Acidification, anoxia, and extinction a multiple regression analysis of extinction selectivity through the Middle and Late Permian: Geology, v. 39, p. 1059–1062, https://doi.org/10.1130/G32230.1.

De Kock, M.O., and Kirschvink, J.L., 2004, Paleomagnetic constraints on the Permian-Triassic boundary in terrestrial strata of the Karoo Supergroup, South Africa: Implications for causes of the End-Permian Extinction Event: Gondwana Research, v. 7, p. 175–183, https://doi.org/10.1016/S1342-937X(05)70316-6.

Duncan, R.A., Hooper, P.R., Rehacek, J., Marsh, J.S., and Duncan, A.R., 1997, The timing and duration of the Karoo igneous event, southern Gondwana: Journal of Geophysical Research, v. 102, p. 18,127–18,138, https://doi.org/10.1029/97JB00972.

Erwin, D.H., 2006, Extinction—How Life on Earth Nearly Ended 250 Million Years Ago: Princeton, N.J., Princeton University Press, 320 p.

Fisher, R.A., 1953, Dispersion on a sphere: Proceedings of the Royal Society of London, v. 217, p. 295–305, https://doi.org/10.1098/rspa.1953.0064.

Flowers, R.M., and Schoene, B., 2010, Mesozoic relief development and uplift of the eastern Kaapvall craton, southern African Plateau from (U-Th)/He thermochronometry: Geology, v. 38, p. 827–830, https://doi.org/10.1130/G30980.1.

Gastaldo, R.A., and Demko, T.M., 2011, Long term hydrology controls the plant fossil record: Topics in Geobiology, v. 32, p. 249–285, https://doi.org/10.1007/978-90-481-8643-3_7.

Gastaldo, R.A., and Neveling, J., 2012, The terrestrial Permian–Triassic boundary event is a nonevent: REPLY: Geology, v. 40, p. e257, https://doi.org/10.1130/G32975Y.1.

Gastaldo, R.A., and Neveling, J., 2016, Comment on: Anatomy of a mass extinction: Sedimentological and taphonomic evidence for drought-induced die-offs at the Permo-Triassic boundary in the main Karoo Basin, South Africa: Palaeogeography, Palaeoclimatology, Palaeoecology, v. 396, p. 99–118, 10.1016/j.palaeo.2014.06.027.

Gastaldo, R.A., and Rolerson, M.W., 2008, *Katbergia* gen. nov., A new trace fossil from the Upper Permian and Lower Triassic Rocks of the Karoo Basin: Implications for paleoenvironmental conditions at the P/Tr extinction event: Palaeontology, v. 51, p. 215–229, https://doi.org/10.1111/j.1475-4983.2007.00743.x.

Gastaldo, R.A., Neveling, J., Clark, C.K., and Newbury, S.S., 2009, The terrestrial Permian-Triassic boundary event bed is a non-event: Geology, v. 37, p. 199–202, https://doi.org/10.1130/G25255A.1.

Gastaldo, R.A., Pludow, B.A., and Neveling, J., 2013, Mud aggregates from the Katberg Formation, South Africa: Additional evidence for Early Triassic degradational landscapes: Journal of Sedimentary Research, v. 83, p. 531–540, https://doi.org/10.2110/jsr.2013.45.

Gastaldo, R.A., Knight, C.L., Neveling, J., and Tabor, N.J., 2014, Latest Permian Paleosols from Wapadsberg Pass, South Africa: Implications for Changhsingian Climate: Geological Society of America Bulletin, v. 126, p. 665–679, https://doi.org/10.1130/B30887.1.

Gastaldo, R.A., Kamo, S.L., Neveling, J., Geissman, J.W., Bamford, M., and Looy, C.V., 2015, Is the vertebrate defined Permian-Triassic boundary in the Karoo Basin, South Africa, the terrestrial expression of the End Permian marine event?: Geology, v. 43, p. 939–942, https://doi.org/10.1130/G37040.1.

Gastaldo, R.A., Neveling, J., Looy, C.V., Bamford, M.K., Kamo, S.L., and Geissman, J.W., 2017, Paleontology of the Blaauwater 67 and 65 Farms, South Africa: Testing the *Daptocephalus/lystrosaurus* biozone boundary in a stratigraphic framework: Palaios, v. 32, p. 349–366, https://doi.org/10.2110/palo.2016.106.

Geissman, J.W., and Ferre, E.C., 2013, Paleomagnetism of Early Jurassic igneous rocks of the Karoo Large Igneous Province, South Africa, and an evaluation of Karoo paleomagnetic data bearing on the recently postulated Jurassic true polar wander event: Geological Society of America Abstracts with Programs, v. 45, no. 7, p. 811.

Gerstenberger, H., and Haase, G., 1997, A highly effective emitter substance for mass spectrometric Pb isotope ration determinations: Chemical Geology, v. 136, p. 309–312, https://doi.org/10.1016/S0009-2541(96)00033-2.

Hancox, P.J., Brandt, D., Reimold, U., Koeberl, C., and Neveling, J., 2002, Permian-Triassic boundary in the northwest Karoo basin: Current stratigraphic placement, implications for basin development models, and the search for evidence of impact, *in* Koeberl, C., and MacLeod, K.G., eds., Catastrophic Events and Mass Extinctions: Impacts and Beyond: Geological Society of America Special Paper 356, p. 429–444, https://doi.org/10.1130/0-8137-2356-6.429.

Hargraves, R.B., Rehacek, J., and Hooper, P.R., 1997, Palaeomagnetism of the Karoo igneous rocks in Southern Africa: South African Journal of Geology, v. 100, p. 195–212.

Hiller, N., and Stavrakis, N., 1980, Distal alluvial fan deposits in the Beaufort Group of the Eastern Cape Province: Transactions, Geological Society of South Africa, v. 83, p. 353–360.

Hiller, N., and Stavrakis, N., 1984, Permo-Triassic fluvial systems in the southeastern Karoo Basin, South Africa: Palaeogeography, Palaeoclimatology, Palaeoecology, v. 45, p. 1–21, https://doi.org/10.1016/0031-0182(84)90106-8.

Hounslow, M.W., and Balabanov, Y.P., 2016, A geomagnetic polarity time scale for the Permian, calibrated to stage boundaries, *in* Lucas, S.G., and Shen, S.Z., eds., The Permian Time Scale: Geological Society of London, Special Publication 450, https://doi.org/10.1144/SP450.8.

Jaffey, A.H., Flynn, K.F., Glendenin, L.E., Bentley, W.C., and Essling, A.M., 1971, Precision measurement of half-lives and specific activities of $^{235}$U and $^{238}$U: Physical Review, v. 4, p. 1889–1906.

Jelinek, V., 1981, Characterization of the magnetic fabrics of rocks: Tectonophysics, v. 79, p. T63–T67, https://doi.org/10.1016/0040-1951(81)90110-4.

Johnson, M.R., Anhaeusser, C.R., and Thomas, R.J., eds., 2006, The Geology of South Africa: The Geological Society of South Africa: Pretoria Johannesburg and the Council for Geoscience, 2nd Edition, 691 p.

Jourdan, F., Feraud, G., Bertrand, H., Bashira Kampunzu, A., Tshoso, G., Watkeys, M.K., and Le Gall, B., 2005, Karoo large igneous province: Brevity, origin, and relation to mass extinction questioned by new $^{40}$Ar/$^{39}$Ar age data: Geology, v. 33, p. 745–748, https://doi.org/10.1130/G21632.1.

Kirschvink, J.L., 1980, The least squares line and plane and the analysis of paleomagnetic data: Geophysical Journal of the Royal Astronomical Society, v. 62, p. 699–718, https://doi.org/10.1111/j.1365-246X.1980.tb02601.x.

Kraus, M.J., and Hasiotis, S.T., 2006, Significance of different modes of rhizolith preservation to interpreting paleoenvironmental and paleohydrologic settings: examples from Paleogene paleosols, Bighorn Basin, Wyoming, USA: Journal of Sedimentary Research, v. 76, p. 633–646, https://doi.org/10.2110/jsr.2006.052.

Krogh, T.E., 1973, A low contamination method for hydrothermal decomposition of zircon and extraction of U and Pb for isotopic age determinations: Geochimica et Cosmochimica Acta, v. 37, p. 485–494, https://doi.org/10.1016/0016-7037(73)90213-5.

Lanci, L., Tohver, E., Wilson, A., and Flint, S., 2013, Upper Permian magnetic stratigraphy of the lower Beaufort group, Karoo basin: Earth and Planetary Science Letters, v. 375, p. 123–134, https://doi.org/10.1016/j.epsl.2013.05.017.

Li, J.W., Gastaldo, R.A., Neveling, J., and Geissman, J.W., 2017, Siltstones across the *Daptocephalus* (*Dicynodon*) and *Lystrosaurus* Assemblage Zones, Karoo Basin, South Africa, show no evidence for aridification: Journal of Sedimentary Research, v. 87, p. 653–671, https://doi.org/10.2110/jsr.2017.35.

Lipshultz, K.R., Gastaldo, R.A., Kamo, S.L., Neveling, J., and Geissman, J.W., 2015, Stratigraphic contextualization of volcanic ash deposited near the Permian-Triassic boundary in the Karoo Basin, South Africa: Geological Society of American, Abstracts with Programs, v. 47, no. 7, p. 569.

Lowrie, W., 1990, Identification of ferromagnetic minerals in a rock by coercivity and unblocking temperature properties: Geophysical Research Letters, v. 17, p. 159–162, https://doi.org/10.1029/GL017i002p00159.

Lucas, S.G., 2010, The Triassic timescale based on non-marine tetrapod biostratigraphy and biochronology, *in* Lucas, S.G., ed., The Triassic Timescale: Geological Society, London, Special Publications, v. 334, p. 447–500, https://doi.org/10.1144/SP334.15

Lucas, S.G., 2017a, Permian tetrapod biochronology, correlation and evolutionary events, *in* Lucas, S.G., and Shen, S.Z., eds., The Permian Timescale: Geological Society, London: Special Publication 450, https://doi.org/10.1144/SP450.12

Lucas, S.G., 2017b, Permian tetrapod extinction events: Earth-Science Reviews, v. 170, p. 31–60, https://doi.org/10.1016/j.earscirev.2017.04.008.

Ludwig, K.R., 2003, User's manual for Isoplot 3.00: A geochronological toolkit for Microsoft Excel: Berkeley Geochronology Center, Special Publication, v. 4, p. 1–71.

MacLeod, K.G., Smith, R.M.H., Koch, P.L., and Ward, P.D., 2000, Timing of mammal-like reptile extinctions across the Permian-Triassic boundary in South Africa: Geology, v. 28, p. 227–230, https://doi.org/10.1130/0091-7613(2000)28<227:TOMREA>2.0.CO;2.

Maré, L.P., De Kock, M.O., Cairncross, B., and Mouri, H., 2014, Application of magnetic geothermometers in sedimentary basins: An example from the western Karoo Basin, South Africa: South African Journal of Geology, v. 117, p. 1–14, https://doi.org/10.2113/gssajg.117.1.1.

Marshall, C., 2005, Comment on "Abrupt and gradual extinction among Late Permian land vertebrates in the Karoo Basin, South Africa": Science, v. 308, p. 1413, https://doi.org/10.1126/science.1110443.

Mattinson, J.M., 2005, Zircon U/Pb chemical abrasion (CA-TIMS) method; combined annealing and multi-step partial dissolution analysis for improved precision and accuracy of zircon ages: Chemical Geology, v. 220, p. 47–66, https://doi.org/10.1016/j.chemgeo.2005.03.011.

McElwain, J.C., and Punyasena, S.W., 2007, Mass extinction events and the plant fossil record: Trends in Ecology & Evolution, v. 22, p. 548–557, https://doi.org/10.1016/j.tree.2007.09.003.

McElwain, J.C., Popa, M.E., Hesselbo, S.P., Haworth, M., and Surlyk, F., 2007, Macroecological responses of terrestrial vegetation to climatic and atmospheric change across the Triassic/Jurassic boundary in East Greenland: Paleobiology, v. 33, p. 547–573, https://doi.org/10.1666/06026.1.

Miall, A.D., 1996, The Geology of Fluvial Deposits: Sedimentary Facies, Basin Analysis and Petroleum Geology: Berlin, Springer-Verlag, 575 p.

Muttoni, G., Dallanave, E., and Channell, J.E.T., 2013, The drift history of Adria and Africa from 280 Ma to Present, Jurassic true polar wander, and zonal climate control on Tethyan sedimentary facies: Palaeogeography, Palaeoclimatology, Palaeoecology, v. 386, p. 415–435, https://doi.org/10.1016/j.palaeo.2013.06.011.

Neveling, J., 2004, Stratigraphic and sedimentological investigation of the contact between the *Lystrosaurus* and the *Cynognathus* assemblage zones (Beaufort Group; Karoo Supergroup): Council for Geosciences Bulletin, v. 137, p. 1–165.

Neveling, J., Gastaldo, R.A., Kamo, S.L., Geissman, J.W., Looy, C.V., and Bamford, M.K., 2016a, A review of

stratigraphic, geochemical, and paleontologic correlations data of the terrestrial end-Permian record in the Karoo Basin, South Africa, *in* de Wit, M., and Linol, B., eds., The Origin and Evolution of the Cape Mountains and Karoo Basin: Springer Publishing, p. 151–157.

Neveling, J., Gastaldo, R.A., and Geissman, J.W., 2016b, Permo–Triassic boundary in the Karoo Basin: Field trip guide Pre-3: Pretoria, South Africa, Council for Geoscience, 81 p. https://doi.org/10.13140/RG.2.2.22414.15683.

Opdyke, N.D., and Channel, J.E.T., 1996, Magnetic Stratigraphy: San Diego, Academic Press, 346 p.

Pace, D.W., Gastaldo, R.A., and Neveling, J., 2009, Early Triassic aggradational and degradational landscapes of the Karoo basin and evidence for climate oscillation following the P-Tr Event: Journal of Sedimentary Research, v. 79, p. 316–331, https://doi.org/10.2110/jsr.2009.036.

Payne, J.L., and Clapham, M.F., 2012, End-Permian mass extinction in the oceans: an ancient analog for the twenty-first century?: Annual Review of Earth and Planetary Sciences, v. 40, p. 89–111, https://doi.org/10.1146/annurev-earth-042711-105329.

Prevec, R., Gastaldo, R.A., Neveling, J., Reid, S.B., and Looy, C.V., 2010, An autochthonous glossopterid flora with latest Permian palynomorphs from the *Dicynodon* Assemblage Zone of the southern Karoo Basin, South Africa: Palaeogeography, Palaeoclimatology, Palaeoecology, v. 292, p. 391–408, https://doi.org/10.1016/j.palaeo.2010.03.052.

Retallack, G.J., Smith, R.H.M., and Ward, P.D., 2003, Vertebrate extinction across Permian-Triassic boundary in Karoo Basin, South Africa: Geological Society of America Bulletin, v. 115, p. 1133–1152, https://doi.org/10.1130/B25215.1.

Roopnarine, P.D., and Angielczyk, K.D., 2015, Community stability and selective extinction during the Permian-Triassic mass extinction: Science, v. 350, p. 90–93, https://doi.org/10.1126/science.aab1371.

Roopnarine, P.D., Angielczyk, K.D., Wang, S.C., and Hertog, R., 2007, Trophic network models explain instability of Early Triassic terrestrial communities: Proceedings of the Royal Society B, v. 274, p. 2077–2086, https://doi.org/10.1098/rspb.2007.0515.

Rubidge, B.S., 1995, Biostratigraphy of the Beaufort Group (Karoo Supergroup): Biostratigraphic series, 35 p.

Rubidge, B.S., Erwin, D.H., Ramezani, J., Bowring, S.A., and de Klerk, W.J., 2013, High-precision temporal calibration of Late Permian vertebrate biostratigraphy: U-Pb zircon constraints from the Karoo Supergroup, South Africa: Geology, v. 41, p. 363–366, https://doi.org/10.1130/G33622.1.

Rubidge, B.S., Day, M.O., Barbolini, N., Hancox, P.J., Choiniere, J., Bamford, M.K., Viglietti, P.A., McPhee, B., and Jirah, S., 2016, Advances in nonmarine Karoo biostratigraphy: Significance for understanding basin development, *in* de Wit, M., and Linol, B., eds., The Origin and Evolution of the Cape Mountains and Karoo Basin: Springer Publishing, p. 141–149.

Sheldon, N.D., 2005, Do red beds indicate paleoclimatic conditions?: A Permian case study: Palaeogeography, Palaeoclimatology, Palaeoecology, v. 228, p. 305–319, https://doi.org/10.1016/j.palaeo.2005.06.009.

Shen, S.-A., et al., 2011, Calibrating the end-Permian mass extinction: Science, v. 334, p. 1367–1372, https://doi.org/10.1126/science.1213454.

Sidor, C.A., Vilhena, D.A., Angielczk, K.D., Huttenlocker, A.K., Nesbitt, S.J., Peecook, B.R., Steyer, J.S., Smith, R.M.H., and Tsuji, L.A., 2013, Provincialization of terrestrial faunas following the end-Permian mass extinction: Proceedings of the National Academy of Sciences of the United States of America, v. 110, p. 8129–8133, https://doi.org/10.1073/pnas.1302323110.

Smith, R.H.M., 1995, Changing fluvial environments across the Permian-Triassic boundary in the Karoo Basin, S. Africa and possible causes of tetrapod extinctions: Palaeogeography, Palaeoclimatology, Palaeoecology, v. 117, p. 81–104, https://doi.org/10.1016/0031-0182(94)00119-S.

Smith, R.H.M., and Botha, J., 2005, The recovery of terrestrial vertebrate diversity in the South African Karoo Basin after the end-Permian extinction: Comptes Rendus Palévol, v. 4, p. 623–636, https://doi.org/10.1016/j.crpv.2005.07.005.

Smith, R.H.M., and Botha-Brink, J., 2014, Anatomy of a mass extinction: Sedimentological and taphonomic evidence for drought-induced die-offs at the Permo-Triassic boundary in the main Karoo Basin, South Africa: Palaeogeography, Palaeoclimatology, Palaeoecology, v. 396, p. 99–118, https://doi.org/10.1016/j.palaeo.2014.01.002.

Smith, R.H.M., and Ward, P.D., 2001, Pattern of vertebrate extinctions across an event bed at the Permian-Triassic boundary in the Karoo Basin of South Africa: Geology, v. 29, p. 1147–1150, https://doi.org/10.1130/0091-7613(2001)029<1147:POVEAA>2.0.CO;2.

Svensen, H., Corfu, F., Polteau, S., Hammer, Ø., and Planke, S., 2012, Rapid emplacement in the Karoo Large Igneous Province: Earth and Planetary Science Letters, v. 325-326, p. 1–9, https://doi.org/10.1016/j.epsl.2012.01.015.

Szurlies, M., 2013, Late Permian (Zechstein) magnetostratigraphy in Western and Central Europe, *in* Gąsiewicz, A., and Słowakiewicz, M., eds., Palaeozoic Climate Cycles: Their Evolutionary and Sedimentological Impact: Geological Society of London Special Publication 376, p. 73–85, https://doi.org/10.1144/SP376.7.

Torsvik, T.H., Van der Voo, R., Preeden, U., Niocalli, C.M., Steinberger, B., Doubrovine, P.V., van Hinsbergen, D.J.J., Domeier, M., Gaina, C., Tohver, E., Meert, J.G., McCausland, P.J.A., and Cocks, L.R.M., 2012, Phanerozoic polar wander, palaeogeography and dynamics: Earth-Science Reviews, v. 114, p. 325–368, https://doi.org/10.1016/j.earscirev.2012.06.007.

Twitchett, R.J., Looy, C.V., Morante, R., Visscher, H., and Wignall, P.B., 2001, Rapid and synchronous collapse of marine and terrestrial ecosystems during the end-Permian mass extinction event: Geology, v. 29, p. 351–354, https://doi.org/10.1130/0091-7613(2001)029<0351:RASCOM>2.0.CO;2.

Van der Voo, R., 1993, Paleomagnetism of the Atlantic, Tethys, and Iapetus Oceans: Cambridge, UK, Cambridge University Press, 411 p, https://doi.org/10.1017/CBO9780511524936.

Viglietti, P.A., Smith, R.H.M., Angielczyk, K.D., Kammerer, C.F., Fröbish, J., and Rubidge, B.S., 2016, The *Daptocephalus* Assemblage Zone (Lopingian), South Africa: a proposed biostratigraphy based on a new compilation of stratigraphic ranges: Journal of African Earth Sciences, v. 113, p. 153–164, https://doi.org/10.1016/j.jafrearsci.2015.10.011.

Viglietti, P.A., Smith, R.H.M., and Rubidge, B.S., 2018, Changing palaeoenvironments and tetrapod populations in the *Daptocephalus* Assemblage Zone (Karoo Basin, South Africa) indicate early onset of the Permo-Triassic mass extinction: Journal of African Earth Sciences, v. 138, p. 102–111, https://doi.org/10.1016/j.jafrearsci.2017.11.010.

Ward, P.D., Montgomery, D.R., and Smith, R.H.M., 2000, Altered river morphology in South Africa related to the Permian-Triassic extinction: Science, v. 289, p. 1740–1743, https://doi.org/10.1126/science.289.5485.1740.

Ward, P.D., Botha, J., Buick, R., DeKock, M.O., Erwin, D.H., Garrison, G., Kirschvink, J., and Smith, R.M.H., 2005, Abrupt and gradual extinction among Late Permian land vertebrates in the Karoo Basin, South Africa: Science, v. 307, p. 709–714, https://doi.org/10.1126/science.1107068.

Ward, P.D., Retallack, G.J., and Smith, R.M.H., 2012, The terrestrial Permian–Triassic boundary event bed is a non-event: COMMENT: Geology, v. 40, p. e256, https://doi.org/10.1130/G31473C.1.

World Magnetic Model, 2010, https://www.ngdc.noaa.gov/geomag/WMM/DoDWMM.shtml.

Zijderveld, J.D.A., 1967, Demagnetization of rocks: Analysis of results, *in* Collinson, D.W., Creer, K.M., and Runcorn, S.K., eds., Methods in Palaeomagnetism: Amsterdam, Elsevier, p. 254, 286.

Science Editor: Bradley S. Singer
Associate Editor: Xixi Zhao

Manuscript Received 7 July 2017
Revised Manuscript Received 30 January 2018
Manuscript Accepted 19 February 2018

Printed in the USA